AN EXPERIMENTAL STUDY OF LIFTING AND MOVING FORCES IN AIR CONVEYING SYSTEMS

by

Sylvaine Chardon

Thesis submitted to the Graduate faculty of the
Virginia Polytechnic Institute and State University
in partial fulfillment of the requirements for the degree of

MASTER OF SCIENCE

in

Mechanical Engineering

APPROVED:

Hal L. Moses, Chairman

James R. Mahan

John Moore

February ,1992

Blacksburg,Virginia

AN EXPERIMENTAL STUDY OF LIFTING AND MOVING FORCES IN AIR CONVEYING SYSTEMS

by

Sylvaine Chardon

Dr. Hal L. Moses, Chairman

Mechanical Engineering

ABSTRACT

An air conveying system uses pressurized air as a propelling force to lift and move articles. It is supplied by a fan into a plenum with a top surface that is a flat perforated plate. Air escapes through the openings, creating a layer that supports and drives the articles along.

This thesis provides information on the lifting and moving forces. It summarizes the results of both analytical and experimental studies. Most of the effort is focused on an experimental procedure for measuring the actual forces on the objects being conveyed and data are used to verify the analytical models.

The experiments are limited to straight holes and louvers located under the bottom of aluminum concave-bottom cans. In some tests, a flat disc has been fixed to the bottom of the cans. Measurements are made of the can motion on an actual section of conveyor.

ACKNOWLEDGEMENTS

I would like to thank Dr. Hal L. Moses who served as my advisor. His support, guidance and criticism were deeply valued and kept me motivated throughout the course of this study.

I wish to express my gratitude to Dr. A. Wicks for his valuable assistance in the choice and the assembling of the strain gages that were used for the experimental work.

The funding of the research was provided by the Center for Innovative Technology, and the Simplimatic Engineering Co. I would like to take the opportunity to thank P. Smith from Simplimatic for his cooperation in providing pieces of equipment, such as an actual section of conveyor. I extend my appreciation to the Mechanical Engineering machine shop, in particular J. Lucas for his technical assistance.

I would like to thank Dr. J. Moore for serving as a member of my committee. I wish to express my sincere thanks to Dr. J. R. Mahan, coordinator of the Exchange Program between the Université de Technologie de Compiègne and the Virginia Polytechnic Institute and State University, that permitted me to enroll in the Master's Program of the Mechanical Engineering Department.

Special thanks to my future husband, Jean-Christophe

Brunet, for his invaluable encouragement throughout this study.

Finally, I wish to thank my family and all my friends for their support and the good time I had with them during my free time.

TABLE OF CONTENTS

LIST OF FIGURES

NOMENCLATURE

A_1	sectional area of hole
A_2	cross-sectional area of the total clearance
A_c	sectional area of the can bottom
c	half of the thickness of the beam
C_d	dimensionless discharge coefficient
C_f	dimensionless friction coefficient
d	width of the product
Dg	drag force
E	modulus of elasticity
E_{OUT}	output voltage of bridge circuit
E_{IN}	input voltage to bridge circuit
ΔE_{OUT}	variation of the output voltage
f	deflection of the beam
F	force created by the fluid flow
GF	strain gage factor or sensitivity
h	clearance between the can bottom and the deck plate
H	clearance set before turning on the air supply
h^*	height of the product
I	moment of inertia
l	half of the length of the beam
L	distance from the can bottom to the beam
m	mass of the product

M	moment created by fluid flow
P_0	supply pressure
P_1	pressure inside the concavity of the can bottom
P_a	ambient pressure
R_1	active strain gage
R_2	active strain gage
R_3	active strain gage
R_4	active strain gage
ΔR_1	fractional change in resistance of R_1
ΔR_2	fractional change in resistance of R_2
ΔR_3	fractional change in resistance of R_3
ΔR_4	fractional change in resistance of R_4
T	torque created by the fluid flow
V_1	jet velocity through the opening
V_2	air velocity escaping the concavity
V_{CAN}	can speed

Greek Letters

ϵ	strain
ρ	density
σ	stress
τ_w	shear stress at the wall

CHAPTER 1

INTRODUCTION

1.1 RATIONALE FOR THE RESEARCH

Expanding automation in manufacturing requires all types of conveying systems, and favors the development of new technologies, such as air conveying. This relatively new system of moving objects with air is, in many cases, succeeding other kinds of conveying systems such as belt conveyors. In fact, it is more competitive in terms of cost effectiveness, reduction of damage to products, and conveying speed. For example, it is used to move empty cans or bottles in the beverage industry; *Kellogg Company* also uses air systems to move packets such as breakfast cereals.

Air conveying system design is difficult since the air flow involved is complex. There are an infinite number of variables involved, such as the possible patterns of the air hole, different shapes of products, etc.. Since few studies have been done so far, present designs are, most of the time, based on direct experimentation or trial and error, and so may not be optimum.

A strictly analytical approach is not feasible. Even though computer codes are being developed to predict three-dimensional unsteady turbulent flows, the complex geometry for an air conveying system would make the computational costs prohibitive to use in design. Furthermore, the calculated results may involve a great deal of uncertainty.

Thus, a research effort is needed that combines both experimental and analytical approaches. The analytical approach will have to make use of flow models that involve characteristic features rather than detailed numerical calculations. The models will need to be based on, and verified by, experimental results.

1.2 THESIS OVERVIEW

This research provides basic understanding of the phenomena involved in air conveying systems and information required for design.

The main objective of this study is to calculate the air flow necessary to lift and move products as a function of their weight and configuration. The analysis will also include effects of two hole patterns, identical to those of the actual conveyor provided by Simplimatic Co. A model of product motion in the conveying system is also developed.

Chapter 1 starts with the rationale for the research

that is relevant in both the present industry and the general advancement of knowledge. In the literature review, a few conveyor designs as well as related studies are presented.

Chapter 2 covers the experimental procedure, which is in two parts. The first part reviews basic Wheatstone bridge theory and presents the arrangement of the strain gages used in the setup to measure flow forces on the products. The second part explains the can conveying speed measurements made on an actual air system with use of microsensors and a high-precision digital counter.

Chapter 3 introduces analytical models for lifting products: one for products with concave bottom shape, and another for products with flat supporting bases. The variables involved are supply pressure, hole size , product supporting area and weight. A model of product motion in the conveying system is presented.

In Chapter 4, the experimental results of the lifting forces on cans and discs are given, as well as those of the moving forces. Curves of the can motion speed on the conveyor are presented. A comparison of the analytical models with the experiments is made.

Conclusions and recommendations are given in Chapter 5.

1.3 LITERATURE REVIEW

Very few technical reports on air conveying systems were found. In the past, firms designed conveyors by trial and error, and did not publish their results. Today, the research done within firms is proprietary. Therefore, neither trade journal references nor patents contain fundamental studies on lifting and moving products with air. However, several devices are described.

As far as experimental and theoretical studies are concerned, J. J. Spillman(1985) published his experimental work on "an improved air-bed conveyor". Basic studies of lifting forces from single and multiple holes are described by Chandra (1987,90). The theory of externally pressurized gas bearings, also developed by Mori, Yabe and Ohnishi (1966,1971), might be applicable in some cases.

1.3.1 AIR CONVEYOR DESIGNS

The large variety of air conveyors shows that each design applies to specific products and applications. Patents provide pieces of information about existing conveyors. They give ranges of air supply pressure, and sometimes values of flow rates, but only for specific products being conveyed.

Air conveyors could be classified into two

categories. In the first category (See Fig 1.a) the plenum chamber is attached to the underside of the conveying table; air jets impinge on the bottom side of the conveyed products so that they ride on a cushion of air. In the second category (See Fig 1.b) the plenum chamber defines an inverted U-shaped conveying channel, such that the air jets go through both vertical sides of the channel, and impinge on the vertical sides of the products in the downstream direction.

Lindstrom (1987) described an example of the first category. His objective was to design a conveying mechanism to transfer cups which are ejected vertically from a cupping press. The system, consisting of parallel conveying tables connected with a plenum, includes an air accelerator hood and a metal sensor at the inlet of each conveying lane. The patent discloses operating ranges for the air supply pressure in each lane of 4 to 8 in. of water (990 to 1980 Pa) and the air flow rate in the duct of approximately 200 SCFM (0.09 m^3/s). The author mentions that "the rate, of course, will vary depending upon the object being moved ", but he does not give any theoretical analysis that could help to calculate new rates. Furthermore, no details about the holes or slots of the conveying lane are given in this document.

Lenhart (1988) invented more complicated air conveying tables for containers. They are an assembly of

- a -

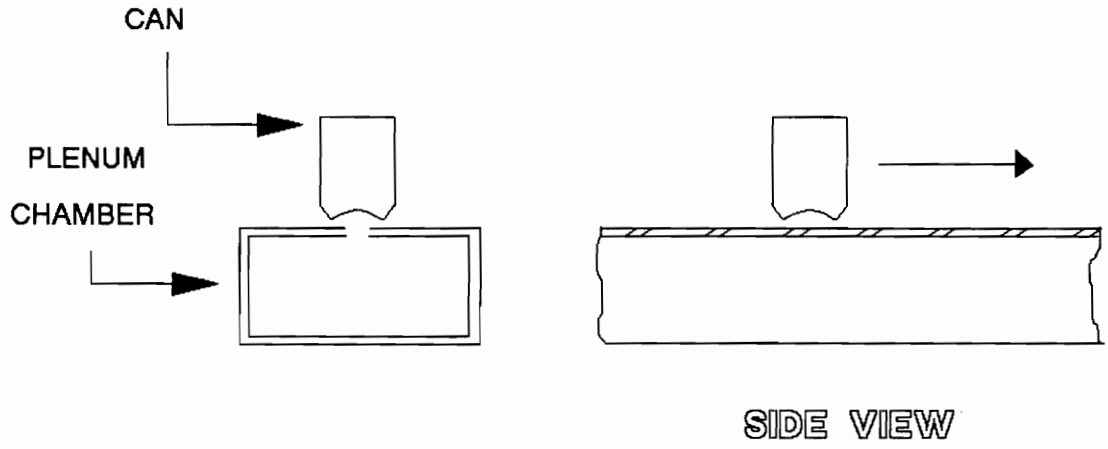

- b -

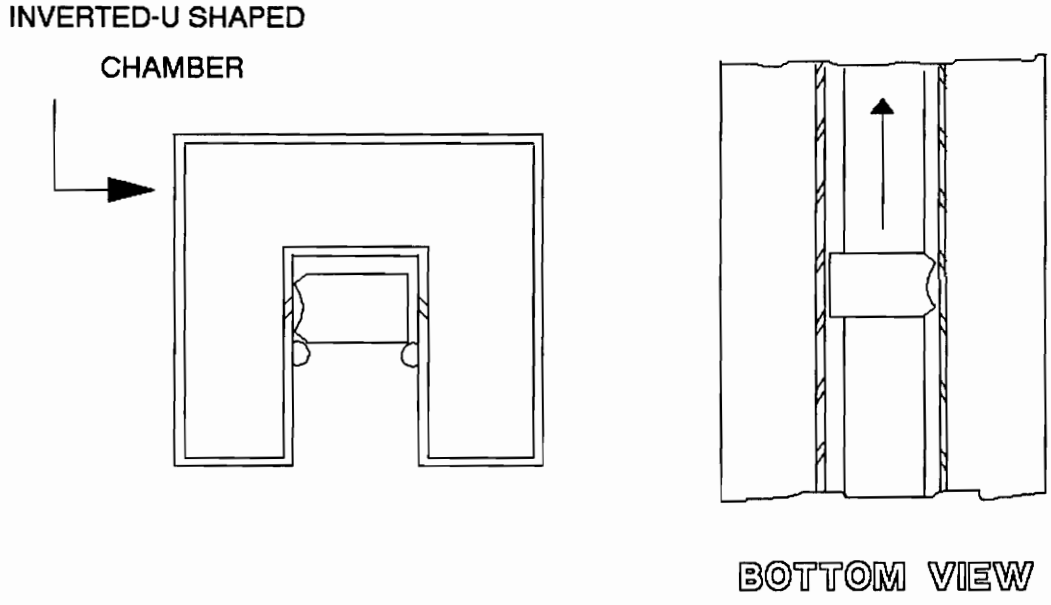

Figure 1 Different Kinds of Conveyors

different conveying sections. At the beginning of the lane, the conveyor supports a mass of containers which are then separated into two independent rows ,and later merge back into a single line. The arrangement of the air jet openings (vertical flotation jets, angled acceleration jets, divergent jets), and the supply pressure are different in each section of the conveyor. The apparatus is also provided with a top covering the section where cans separate into two rows along the side walls of the conveying table. A longitudinal row of driving jets positioned along each edge of the top cover maintains the containers in the upright position. Then, the two rows are "brought into nesting relationship and into a triangular equilateral configuration". Acceleration jets and converging walls generate a high-pressure zone which transforms the triangle configuration into a single line configuration. For this conveyor, different jets are used (5/64, 7/64, 3/16 in. in diameter - 2, 2.8, 4.8 mm) at different angles(from 5° to 60° from the vertical). Depending on the plenum sections, Lenhart found a pressure of approximately 1 in. to 5 in. of water (250 to 1250 Pa) "to be satisfactory".

In the two preceding patent documents, the connection between the blower and the plenum chamber was not shown. Futer (1983), however, considers it as a main feature in the conveyor design.

The surface flow air conveyor, designed by Futer,

has an open wheel fan mounted within the plenum. The plenum communicates with the conveying surface; it is formed with a pod opening which enables the supply air pressurized by the fan to move upstream as well as downstream. The inventor claims that this new configuration of air supply yields better pressurization compared to conveyors with the wheel fan mounted in a scroll housing outside the plenum. The new structure results "in an increase in pressure from 1.9 inches of water gauge to 2.4 inches of water gauge in one example test installation".

Others positive aspects are the reduction of the construction cost, the use of smaller electric motors, the mass production of modular sections of air conveying tables with plenums, which pod housings can be attached to, and the possibility to connect modular sections together.

This document, however contains no details about the conveying surface, said to be formed with Coanda-effect directional openings.

The conveyor invented by Lenhart (1983) illustrates the second category of conveying systems. The apparatus makes use of slanted air jets applied above the central line of the aluminum cans lying perpendicular to the downstream direction. The conveyor operates a horizontal transfer with no can-to-can contact on an inverted-U channel; i.e, whose top is closed and bottom is open.

A plenum chamber is attached to both vertical side walls of the channel, and air at a positive static pressure is forced through the slanted jet openings of the side walls into the U-shaped channel. To move containers apart from each other at a certain speed requires a pressure above and between the containers, at least 0.02 in. of water (5 Pa) greater than the ambient pressure . To maintain this condition, the size and the angle of the jet openings and the supply pressure in the plenum will be adjusted each time a different object is being conveyed.

The patent document provides tables of data (can train speed, average air jet velocity, separation between the cans, etc.) for different values of angle jet, size jet, and supply pressure when operating with twelve fluid aluminum cans. For example, the best operation has been obtained with a 5/16 in. (8 mm) diameter jet at an angle of 9° from the horizontal, an air flow rate per jet of 1.85 CFM (8.7×10^{-4} m^3/s), a static pressure of one inch of water (250 Pa) at the open end of the cans, and 1.3 in. water (325 Pa) at the closed end. This results in an average jet vector transport velocity of 555 ft/min (2.8 m/s), a delivery of 950 cans per minute with a speed of 216 ft/min (1 m/s) for the can train.

But, those results cannot be used for another kind of container. Moreover, the patent document does not contain any theoretical analysis that could help to calculate the new speed of a different weight object in the same operating

conditions, or determine the operating conditions providing the required speed.

A similar apparatus has been invented by Danler, et al.(1981), but for a different shaped container. In fact, it moves rounded bottom bottles that cannot be conveyed on air cushion tables. An air flow is still used as a propelling force. Bottles are suspended by their necks from suitable guide rails and are moved along the guide rails by overhead jets. As in the case of the previously described device, air comes from the side walls of the inverted U-shaped channel defined by the plenum. Instead of slanted jets, the plenum supplies air to a plurality of slots vertically oriented and lying in a row, along the length of the channel side walls. Thus, air jets are impinging on the neck portion of the bottles. The conveyor is also provided with side walls or curtain members extending along each side of the conveyed bottles so that they define a channel to confine the residual air that aids the directional air in moving the bottles. The patent disclosure does not contain experimental data for speed rates; it only mentions that the supply pressure in the plenum is about 5 in. of water (1250 Pa).

In a word, these patents overview some of the numerous conveying apparatus designs. We notice that the usual operating air pressure is a few inches of water and the hole

diameters do not exceed approximately 5/16 in. (8 mm). We have, so far, no information about the use of slots; however, much more information about the flow pattern is described in the next section.

1.3.2 EXPERIMENTAL STUDIES OF AIR-BED CONVEYING SYSTEMS

In preliminary experimental studies, Spillman (1985) described the flow behavior beneath a circular flat disc, and beneath rectangular base packets for different air-jet opening configurations. He develops a few formulae for the friction drag and momentum. He also calculates the length and the depth of the duct such that the constant axial air velocity and static pressure remain constant along the length of the duct.

The flow behavior beneath a circular flat disc is described first. Air flows through a central hole drilled in a parallel supporting surface, which is set at different heights under the disc. The supply pressure is about 100,000 Pa (40 in. of water). The results show that the pressure distribution depends substantially on the gap size between the disc and the supporting surface. Two opposite effects influence the pressure distribution. Friction creates a loss in static pressure, whereas the increase of cross-sectional area with increase of radius generates expansion effects.

Friction effects dominate for gap sizes from 0.002 to 0.005 in. (0.05 mm - 0.13 mm), while for bigger gaps (0.010 in. - 0.015 in., 0.25 mm - 0.4 mm), an increase of pressure is seen in the inner part of the disc. Although the author claims that the pressure drop is well predicted by a theoretical analysis using air flow rates and friction coefficients, there are no derivations in this paper.

In the case of large flow at the sharp-edged hole, a large pressure drop occurs just downstream the hole as the flow separates. In fact, friction and turbulence in this area cause a large pressure drop. Since they cannot be quantified, the actual volume flow is not that predicted by the theory. The higher the gap height, the higher the flow rate , but the smaller the supported weight. For example, no package of any weight can float at a height greater than 0.015 in. (0.4 mm) with an air supply pressure of 40 in. of water (100,000 Pa).

Instead of a single hole, a row of closely pitched holes was tested as well as two parallel rows to support a rectangular plate. Air escapes from the front and the back of the plate. The pressure losses at the inner edge is less than at the outer edge because the flow between the rows is smaller than that at the outer edge of the holes. For this reason, there is a plateau of high static pressure between the two rows except at the front and the back of the plate. This provides a greater load-carrying capacity than that with only one row.

To make the construction of the conveyor more simple, two longitudinal slots were tested. The slots are slanted inward at angles of about 20°, so that the volume flow required to maintain a given central pressure is reduced. To get the maximum support, the ratio of the distance between slots to the plate width has to be 0.9; the pressure required for this configuration is 43 percent of that required when using two rows of holes near the center-line. Thus, the power required is also less, 60 percent of that for the holes. Another way to reduce the flow is to diminish the clearance at the sides of the floating packet. It is important to realize that the flow rate is dependent on the number of packets covering the slots. For example, the flow rate will decrease as the fraction of length of covered slots increases; but, if it decreases, the pressure inside the duct increases.

The ratio of the axial component of air velocity to the plate velocity has been derived. It is a function of the gap height, the volume flow rate and the drag coefficient which includes the thrust effect of the air escaping from the uncovered slots, the suction effect from the slots ahead, and the friction and the eddy drag of the object. Obviously, the axial component of the air velocity must be greater than the plate speed. It increases when the floating height decreases.

To maintain a constant air-duct velocity, the author proposed a duct cross-sectional area which tapers from the inlet of the duct to the outlet. Depth and length formula are

given as a function of the required fan delivery volume flow rate and the required pressure.

To conclude, Spillman ended up with an "improved air-bed conveyor" provided with slots to reduce construction and operating costs. He mentioned some theoretical analysis, but he admitted that problems of tilting, for example, cannot be predicted, and "tests must be made to check satisfactory propulsion characteristics".

The center of gravity of the package may not necessarily coincide with its axis of symmetry. This generates the effect of tilting of a package relative to the supporting surface. The air film has a variable thickness, both in the transversal and the longitudinal direction. Tilting effects are taken into account by Chandra (1987,88,89) in his studies of an air-film conveyor pressurized through single holes, multiple holes, or parallel slots.

Chandra introduced a variable air-film thickness $h_{x,y}$ in the Reynolds equation governing the pressure distribution in an externally pressurized air film,

$$\frac{\delta}{\delta x}\left(h_{x,y}^3 \frac{\delta P}{\delta x}\right) + \frac{\delta}{\delta y}\left(h_{x,y}^3 \frac{\delta P}{\delta y}\right) = 0 \quad . \qquad (1)$$

To solve Eq. 1 and the boundary condition equations requires use of the finite element method. Thus, using a discretization form of Eq. 1 and experimental correlations for

the recovery pressure in the converging portion and in the diverging portion of the air film, Chandra calculated the pressure distribution, the volume flow rate, and the load capacity for different supply hole patterns.

The results show that the load capacity decreases with an increase in air film thickness, while the volume flow rate increases. On the other hand, it increases with the number of holes, but with an increase in the air requirement per unit load. "A single hole appears to be the most efficient from the point of view of utilization of the air and power supplied, as it has the smallest value of volume flow rate per unit of load lifting capacity when compared to the other cases. Air supply through peripheral holes has a tendency to increase the air requirement with much less increase in the lifting capacity."

As far as the tilting effects are concerned, the decrease of pressure towards the edge of the package flat surface is steeper in the diverging portion of the air film, whereas the pressure drop is more gradual beyond the outer holes in the case of the converging portion of the air film.

The analysis provides pieces of information on load-lifting air films, but not on load-carrying air films since the momentum effects of a package being conveyed have not been taken into account.

We make the same critical observation about the "theoretical flow models of externally pressurized gas

bearings" investigated by Mori, Yabe,and Ohnishi (1966-71); they used potential flow to solve for the pressure distribution in parallel air films of uniform thickness in the case of circular or rectangular load base.

To conclude, the technical literature on air conveying systems is very limited because part of it is proprietary, and not much research has been done so far. It should be noted that the experimental technique of the present research has never been used before.

CHAPTER 2

EXPERIMENTAL PROCEDURE

An experimental apparatus has been designed to measure the forces applied on products being conveyed. For the motion speed measurements experiments were conducted on a real conveyor.

2.1 EQUIPMENT DESCRIPTION FOR FORCE MEASUREMENTS

The basic principle of air conveying systems is to transport packages, cartons, cans, etc., on a thin film of air. Air flow through the openings of the conveyor track generates the air cushion of the conveyor track. Many forms and configurations of hole or slot openings exist; however, we limit our study to a single circular straight hole and a single slanted opening (See Fig 2). The air flow coming out will be different in the two cases. A straight hole generates a lifting force only, while a slanted opening develops also a directional moving force. One of the objectives of the research is to provide basic information on these forces. A system has been designed to simulate the air flow and to

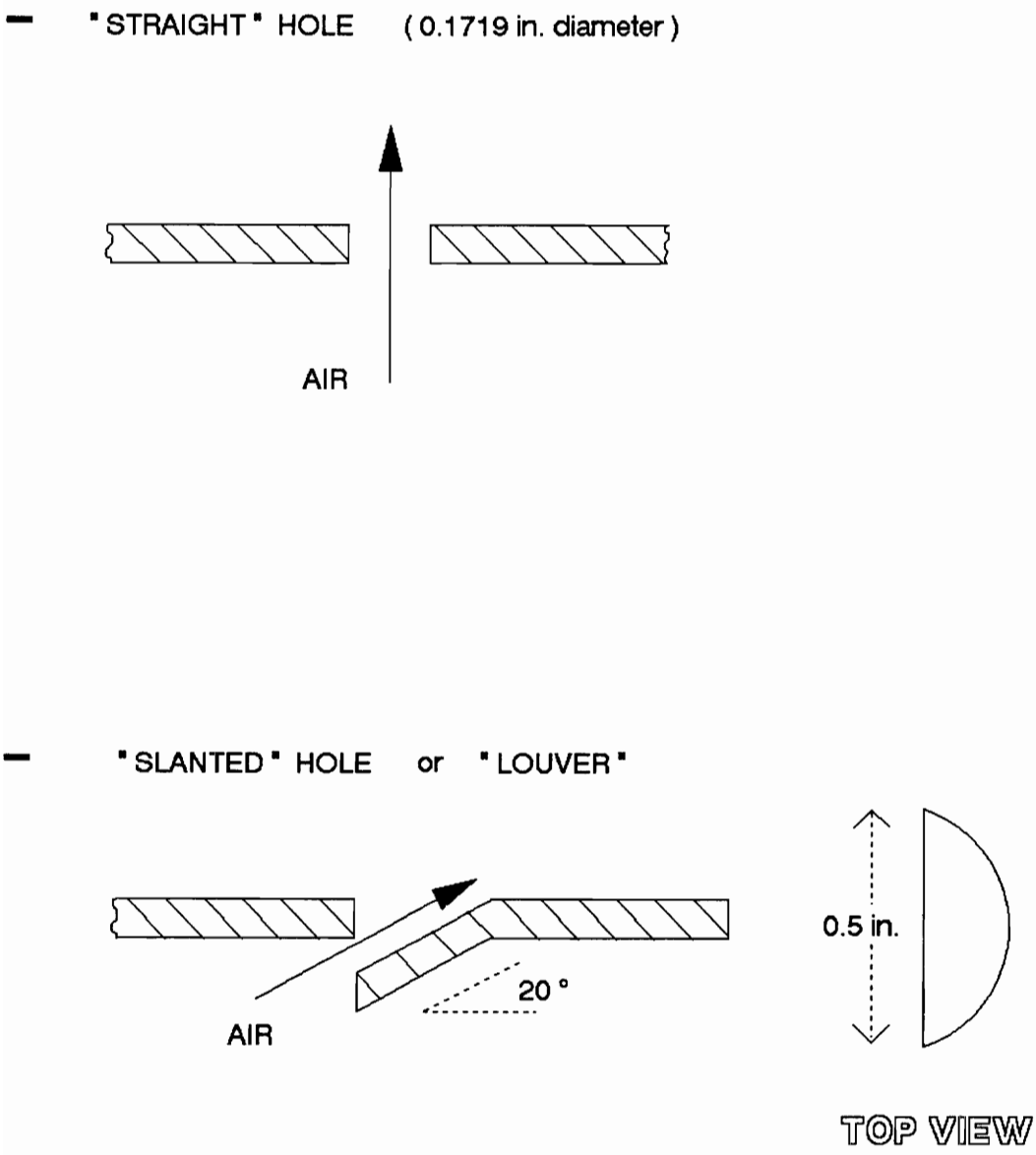

Figure 2 Hole Shapes

measure small forces (1 gram-force - 0.0098 N) with an arrangement of very sensitive strain gages.

2.1.1 BASIC ARRANGEMENT

The air supply box, shown in Fig. 3, was built with a removable top surface to simulate the flow under the object. The clearance between the box and the tested object is adjusted with micrometers as explained in section 2.1.4. In the present case, an empty aluminum can is attached to a horizontal fixed-end beam. The strain in the beam is measured with very sensitive strain gages. The deformation is proportional to the applied force and the corresponding torque created by the fluid flow issuing from a single hole. Figure 4 shows the forces in the case of a single circular hole. The dimensions of the aluminum beam were selected for the following condition: a 1 gram-force (0.0098 N) corresponds to 1 microstrain in the beam. Stress, strain and moment of inertia are calculated to know the beam dimensions (length: 12.5 in. (31.8 mm), width: 0.75 in. (1.9 cm), thickness: 0.05 in. (1.3 mm)).

Two semi conductor strain gages are fixed at each end of the beam as shown in Fig. 5.a, one on the top and one on the bottom. The change of resistance is proportional to the applied force under the can. The strain gages are wired in a

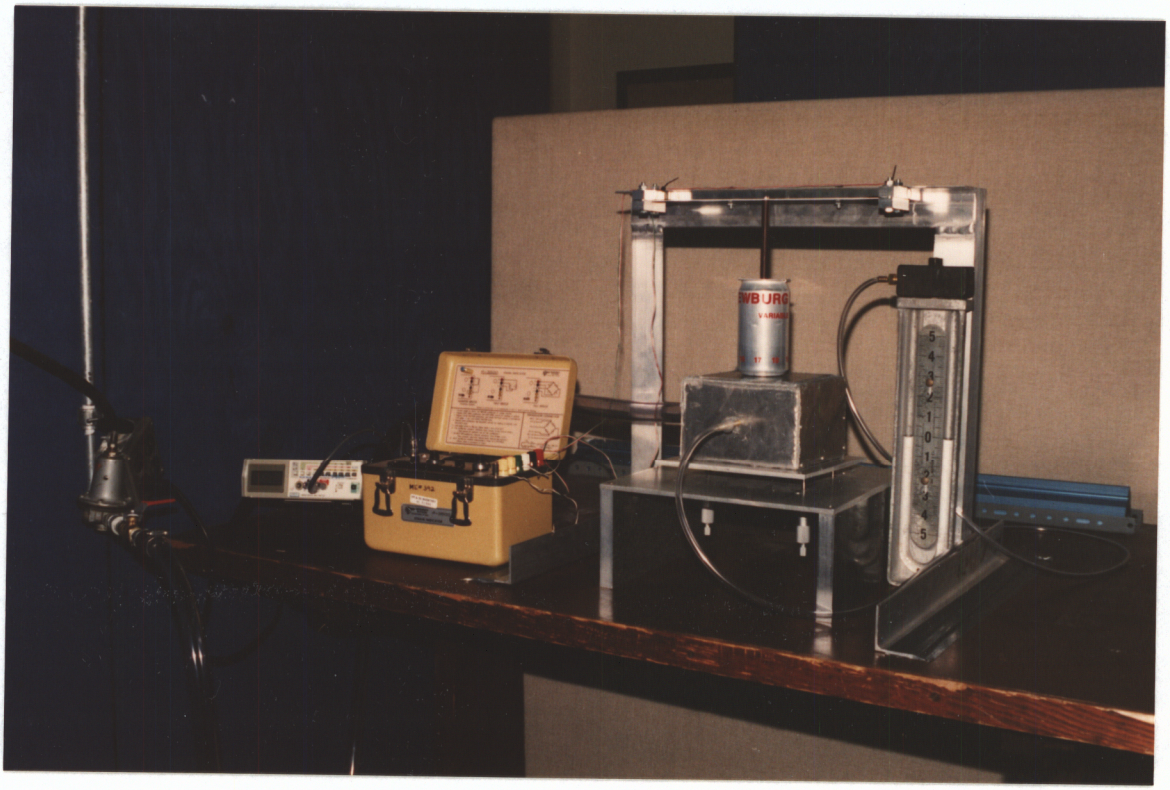

Figure 3 Experimental Arrangement for Forces Measurements

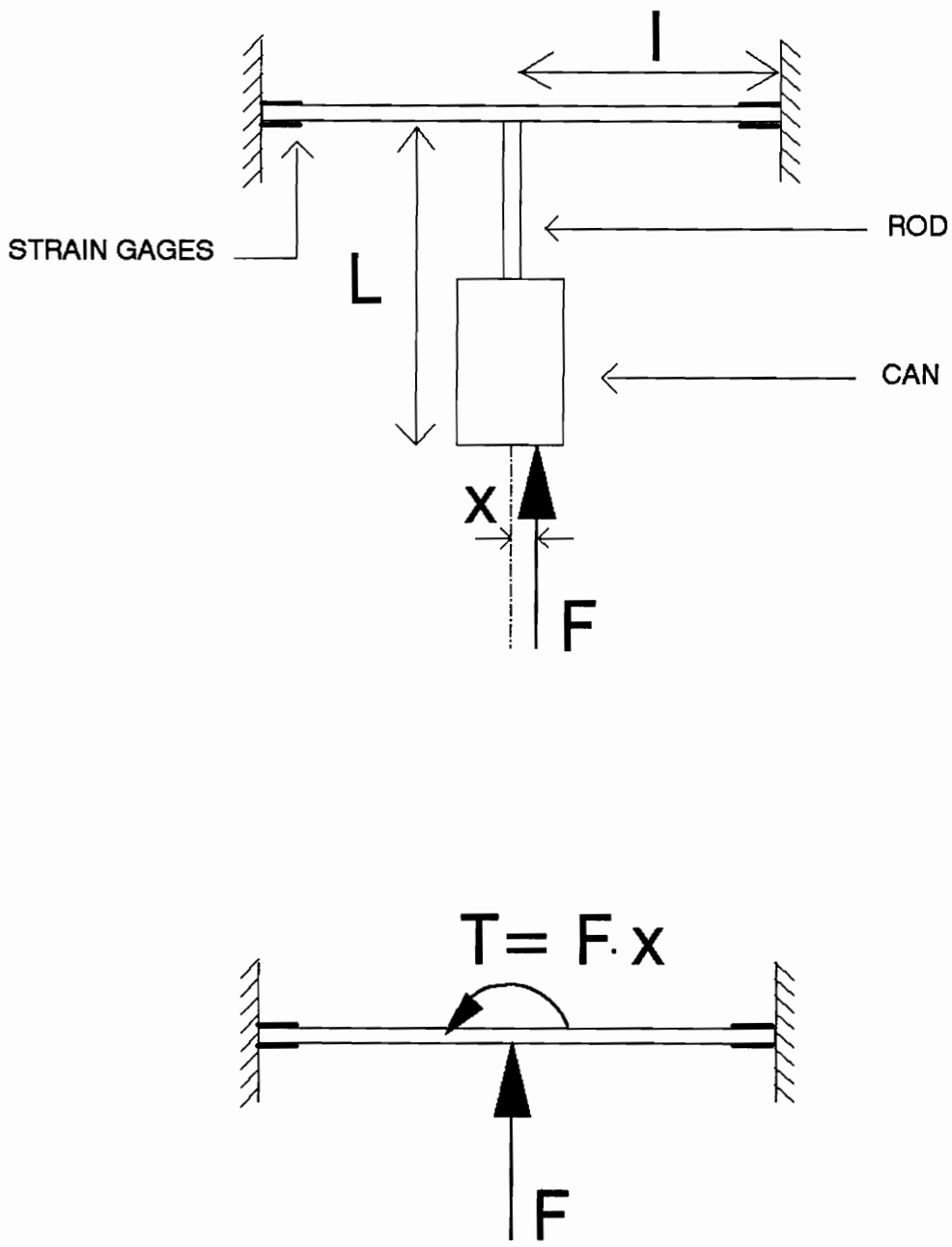

Figure 4 Representation of the Forces from a Single Hole

Wheatstone bridge circuit integrated in a PC-3500 strain indicator. The bridge can be balanced manually. A multimeter connected to the PC-3500 displays the output voltage of the bridge. A calibration of the strain gages correlates the output voltage level to the applied force levels.

In order to differentiate the force measurements from the torque measurements, two different ways of connecting the strain gages in the Wheatstone full-bridge circuit are needed.

2.1.2 WHEATSTONE BRIDGE ARRANGEMENT

The use of some type of bridge circuit is the most common method to convert a signal produced by resistive transducers, such as strain gages, to a useful form. The Wheatstone bridge configuration has been chosen because of its ability to precisely measure small resistance changes. Because the PC-3500 strain indicator already contains a Wheatstone bridge, we use it and "replace" the resistors with active strain gages. The basic configuration of this bridge is shown in Fig. 5.b. The strain gages are excited with a voltage E_{in}, applied across one diagonal, and the output voltage E_{out} is measured across the other diagonal. Using some simple mathematics and electrical laws leads to

-a-

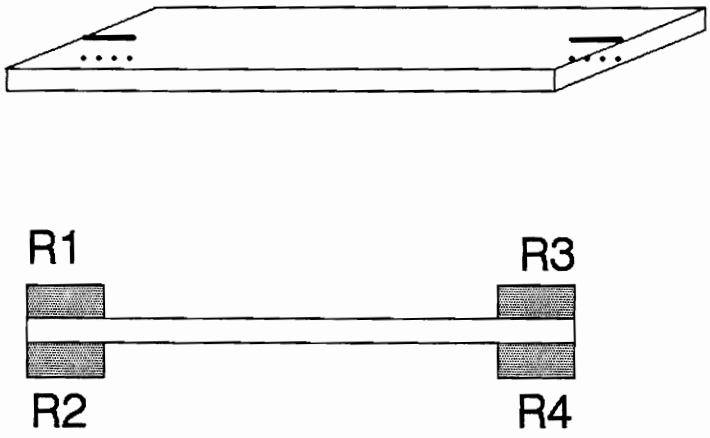

-b-

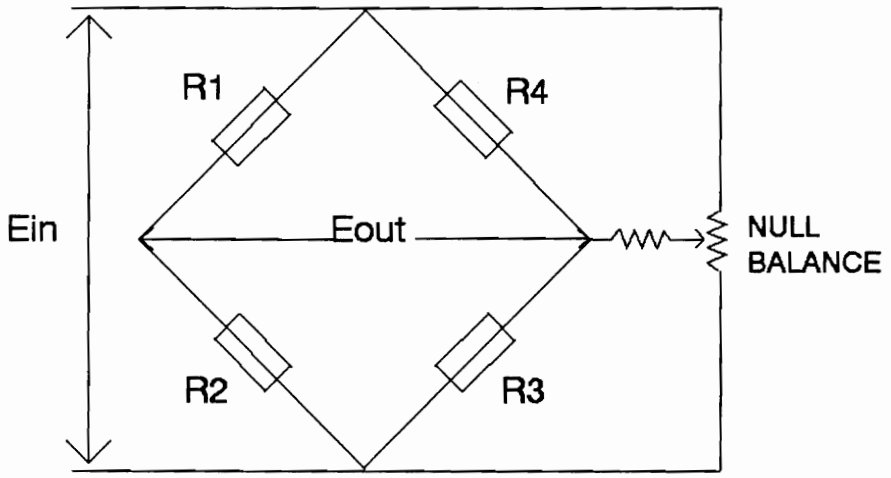

Figure 5 a-Strain Gage Arrangement
b-Wheatstone Bridge Circuit

$$E_{out}=E_{in}\cdot\frac{(R_1R_3-R_2R_4)}{(R_1+R_2)\,.\,(R_3+R_4)} \quad . \tag{2}$$

The condition for balance is

$$R_1R_3=R_2R_4 \quad . \tag{3}$$

Although the four semiconductor strain gages, bonded on the beam, have the same nominal resistance of 350.0 Ω ± 0.3%, the Wheatstone bridge must be balanced since it is much easier to measure small values of ΔE_{out} from a zero voltage base than directly from E_{out}. The instrumentation provides manual balancing that simplifies everything.

When a force is applied on the beam, resistances R_1, R_2, R_3 and R_4 have a variation of ΔR_1, ΔR_2, ΔR_3, ΔR_4, respectively. The change in output voltage is given by

$$\Delta E_{OUT}=E_{IN}\cdot\frac{(R_1+\Delta R_1)\,(R_3+\Delta R_3)-(R_2+\Delta R_2)\,(R_4+\Delta R_4)}{(R_1+\Delta R_1+R_2+\Delta R_2)\,.\,(R_3+\Delta R_3+R_4+\Delta R_4)} \quad . \tag{4}$$

This equation is simplified by assuming that all of the resistances are the same and by neglecting higher order terms. This leads to

$$\Delta E_{OUT}=\frac{E_{IN}}{4R}\,.\,(\Delta R_4+\Delta R_2-\Delta R_1-\Delta R_3) \quad . \tag{5}$$

Referring to Fig. 5.b and Eq. 5, one notes that ΔE_{out} increases in proportion to the algebraic sum of changes in resistance in two opposite arms and in proportion to the

algebraic difference of changes in resistance in two adjacent bridge arms. By different arrangements of bridge connections, either the force effects or the torque effects can be eliminated.

2.1.3 BEAM DEFORMATION MEASUREMENTS

2.1.3.1 LIFTING FORCE

A vertical force pushes the beam up, while the moment created by the fluid flow deforms the beam differently. The deformations are represented with exaggeration in Fig. 6. In the first case, both top strain gages are in compression and both bottom strain gages are in tension. In the second case, one of the top strain gages is in tension and the other one in compression, and vice versa for both bottom gages. To distinguish the force effects from the torque effects requires different bridge circuits. In both cases, both resistance variations due to tension have to be added and subtracted from both resistance changes due to compression.

According to the bridge circuit characteristics, the two deformations can be measured separately. Figure 4 reveals two distinct arrangements. The first only measures the amplitude of the force. Indeed, the changes in resistance due

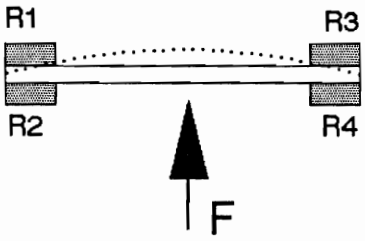

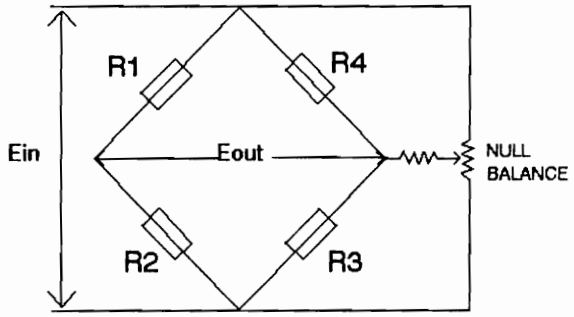

CIRCUIT 1

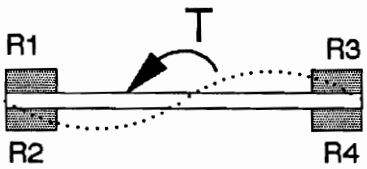

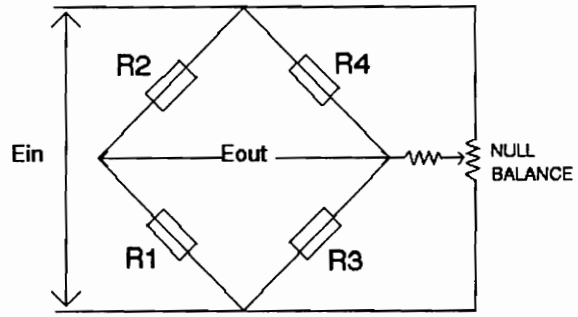

CIRCUIT 2

Figure 6 Circuits for Forces and Torque Measurements

to the torque effects cancel, and vice versa for the other one.

This method can be proved analytically by expressing the four resistance variations in terms of moments, forces, and length.

The stress, σ, at any point of the beam due to an applied force or moment can be written as

$$\sigma = \frac{Mc}{I} \quad , \tag{6}$$

where c is half of the thickness of the beam, I is the area moment of inertia of the beam, and M is the moment created by the fluid flow. Using Hooke's law, the strain at any point of the beam is given by

$$\varepsilon = \frac{Mc}{IE} \quad , \tag{7}$$

where E is the modulus of elasticity of the beam material. The strain can also be expressed in terms of changes in resistance; that is

$$\varepsilon = \frac{\Delta R}{R} / (GF) \quad , \tag{8}$$

where GF is the gage factor of the strain gage. Finally, by equating Eqs. 7 and 8, the change in resistance of any strain gage can be expressed as

$$\Delta R = R(GF)\frac{Mc}{IE} \quad . \tag{9}$$

Recalling the beam deformations, shown in Fig. 6, caused by the vertical force F, shown in Fig. 4, the changes in resistance of the four gages are

$$\Delta R_1 = -R_1 (GF) \frac{F(l+x)c}{IE} \quad , \tag{10}$$

$$\Delta R_3 = -R_3 (GF) \frac{F(l-x)c}{IE} \quad , \tag{11}$$

$$\Delta R_2 = R_2 (GF) \frac{F(l+x)c}{IE} \quad , \tag{12}$$

and

$$\Delta R_4 = R_4 (GF) \frac{F(l-x)c}{IE} \quad . \tag{13}$$

The output voltage of circuit 1, shown in Fig. 6, is given by

$$\Delta E_{OUT} = \frac{E_{IN}}{4R} (\Delta R_4 + \Delta R_2 - \Delta R_1 - \Delta R_3) \quad . \tag{14}$$

Substituting Eqs. 10 through 13 into Eq. 14 leads to a formula for the output voltage that is independent of the moment F.x:

$$\Delta E_{OUT} = E_{IN} \frac{c}{IE} Fl \quad . \tag{15}$$

A similar derivation using appropriate expressions for ΔR1, ΔR2, ΔR3, ΔR4 and ΔE_{out} of the second circuit

proves that changes in resistance due to the upward deformation are canceled if the gages are in the configuration of circuit 2.

2.1.3.2 OBLIQUE FORCE

As we operate with a slanted jet, the flow is obviously different from that from a circular straight hole. The three-dimensional air flow is considered as a two-dimensional flow under the can. Blown air lifts the can and tends to move it in the jet direction. The force has been decomposed into two forces F_x and F_z as shown in Fig. 7.

The vertical force F_z will be measured as explained in the previous paragraph, i.e, wiring the strain gage in the full-bridge Wheatstone circuit 1 as shown in Fig. 6.

It is more complex to determine the amplitude of F_x. Since the strain gages have been set longitudinally along the length of the beam, they cannot accurately detect the longitudinal beam deformation due to F_x. However, the deformation induced by the corresponding torque can be detected by means of the strain gages wired in the full-bridge circuit 2 (See Fig. 6).

Nevertheless, the location of the hole beneath the can is significant. If the hole center is placed anywhere under the can centerline perpendicular to the beam, the output voltage of the circuit barely corresponds to the torque

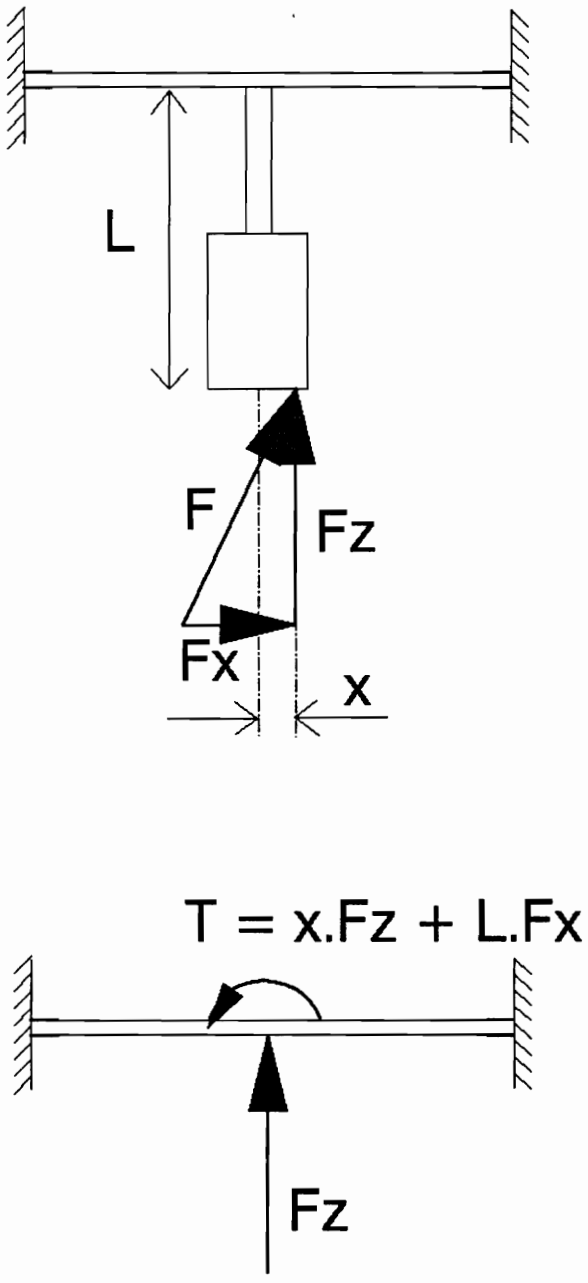

Figure 7 Oblique Force

effects due to F_x. The other configuration is when the hole under the can is placed anywhere on the can centerline parallel to the beam; the gauged torque, then, is the sum of both torque due to F_x and F_z. To distinguish one from the other requires operation with the same experimental conditions but with another known length of supporting rod, so that it will affect only the torque due to F_x. The amplitude of F_x and F_z will be the same because the air flow is the same. Since the moment $F_z.x$ stays approximately the same, F_x can be obtained from Eq. 16:

$$F_x = \frac{(T_1 - T_2)}{(L_1 - L_2)} \quad , \tag{16}$$

where T_1 and T_2 are the respective measured torque in both experiments.

2.1.3.3 FORCE PERPENDICULAR TO THE MOVING DIRECTION

Considering a three-dimensional flow escaping from the inclined opening, information is required about the component $F_{y,}$ perpendicular to F_x and F_z (See Fig. 8). We still use the setup with the strain gages. However, if the beam remains parallel to the flow direction, the original arrangement of strain gages on the beam is inappropriate to detect either the y-direction deformation due to F_y or the

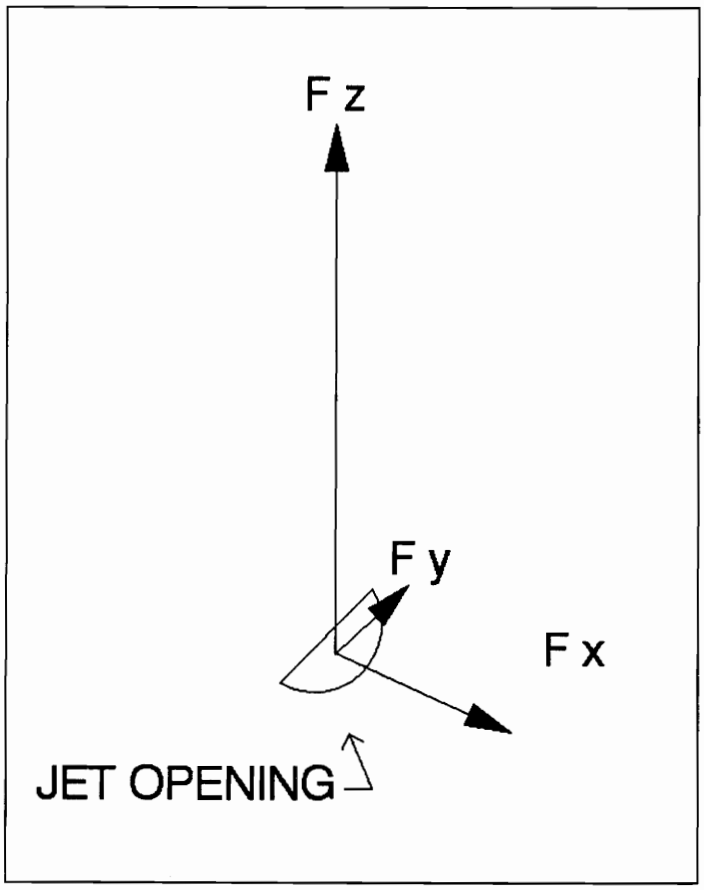

Figure 8 Three-Dimensional Flow Representation

associated torque. The entire support is positioned such that the beam is perpendicular to the flow direction, i.e, parallel to F_y. In this configuration, the strain gages wired in the full-bridge circuit 2 measure the moment $F_y.L$. Depending on the hole position under the can, torque measurements may or may not include the lifting torque effects.

2.1.4 DETERMINATION OF THE CLEARANCE BETWEEN THE CAN BOTTOM AND THE DECK PLATE

A set of three micrometers shown in Fig.1 supports a plate on which the air supply box is mounted. The micrometer resolution is 1/1000 in.

Since the lifting force directly depends on the floating height of the object, we need to know very precisely the clearance between the can bottom surface and the box top surface.

The micrometer position is set by hand. The most difficult part is to obtain the "zero-clearance". The can is fixed and does not touch the top of the air supply box; the output voltage of the instrumentation is set to zero. The three micrometers are moved up, one after the other, until the strain gages detect a tiny deformation of the beam due to a contact between the can bottom and the box which induces a change in the output voltage.

One notes from Fig. 9 that the exact clearance h is the gap H, set up before turning the air supply on, plus the beam deflection f induced by the lifting force F_z when air supply has been turned on.

Thus, the total clearance is

$$h=H+f \quad . \tag{17}$$

Indeed, under the action of the applied force F_z, the beam deflects from its initial position. Since the beam ends have fixed supports, we need to refer to statically indeterminate beam problems to solve for the beam deflection.

The deflection is calculated from (Marks' Standard Handbook for Mechanical Engineers,1978)

$$f=\frac{F}{EI}\frac{(2l)^3}{192} \quad , \tag{18}$$

where F is the amplitude of the applied force , l is half of the length of the beam, I is the moment of inertia and E is the modulus of elasticity.

A clearance h will correspond to each value of F_z. This height is the actual "floating height" of a conveyed object which has a weight of F_z.

2.1.5 STATIC CALIBRATION PROCEDURE

The strain gages require calibration to relate the

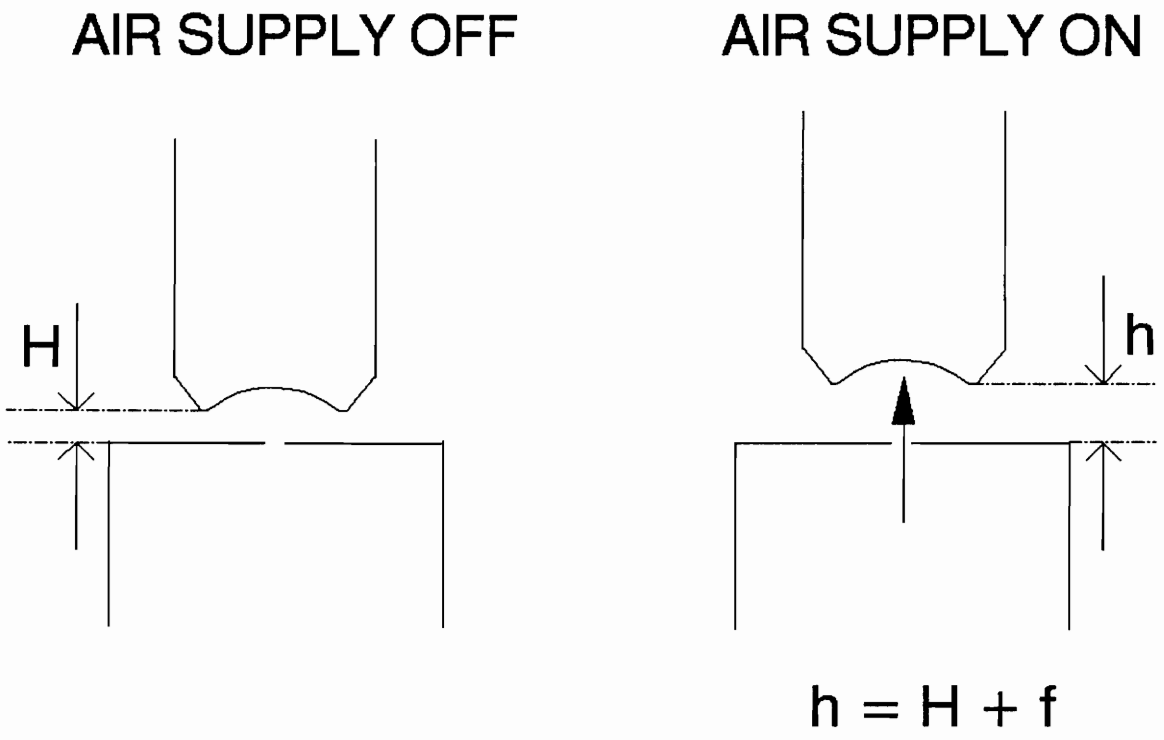

Figure 9 Clearance Between the Can and the Box-Top Surface

instrumentation output voltage level to force levels. The static calibration is performed by hanging weights from the center of the beam. The output voltage is recorded each time a static load is added during the calibration. The static load is plotted versus output voltage. Since the linearity of the gages is very acceptable, results of a linear regression analysis can be used to convert the instrumentation output voltage to force level.

To relate the output voltage to the torque applied to the beam, the calibration of the strain gages is done by turning the whole support. Thus, the beam is vertical, and a rod was fixed perpendicularly at its center. Then, weights were hung from the end of the rod.

2.2 EQUIPMENT DESCRIPTION FOR SPEED MEASUREMENTS

One of the objectives was to determine the actual speed of the cans along an actual air supply and distribution system.

2.2.1 THE AIR CONVEYING APPARATUS

The experiments to measure the speed of cans were conducted on an air conveying system provided by *Simplimatic*

Company, Lynchburg, VA. The conveyor is shown in Fig. 10. The present system uses a commercial fan rotor mounted in a pod, without a casing or scroll, and a single baffle plate to distribute the flow in the plenum chamber.

A scroll housing has been tested, but results do not show significant change in the fan characteristics.

The deck plate above the plenum chamber is a sheet of metal formed with a regular pattern of two kinds of openings: holes and directional slits.

Two guiding rails and a drilled top surface prevent the cans from exiting the conveyor track.

2.2.2 INSTRUMENTATION FOR SPEED MEASUREMENTS

The main idea is to measure the elapsed time between two positions of one can moving on an air film along the conveyor. The apparatus is composed of two sets of microsensors connected to a high resolution counter.

The two sets are positioned and fixed apart on the two side guides of the conveyor. For each set, an infra-red light source is fixed in front of the receiving sensor so that when the can passes through the signal is interrupted and the counter is triggered. The operating chart is shown in Fig.11.

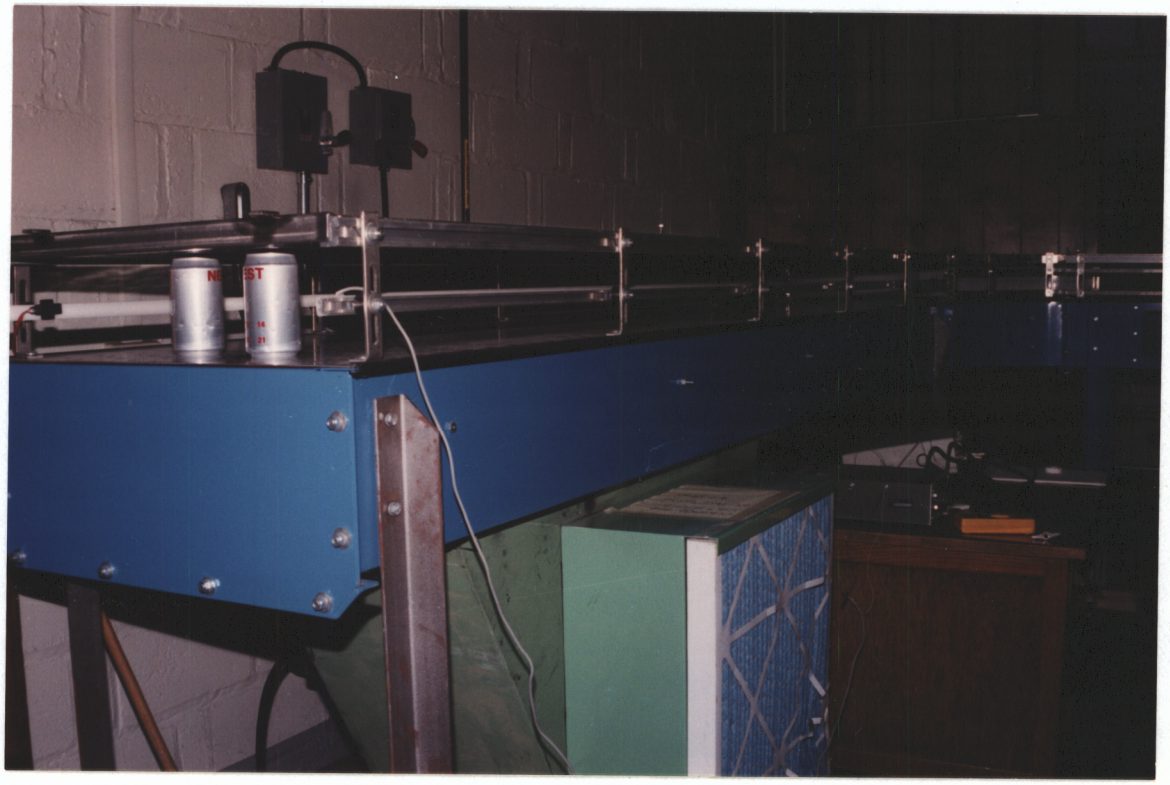

Figure 10 Simplimatic Air Conveyor

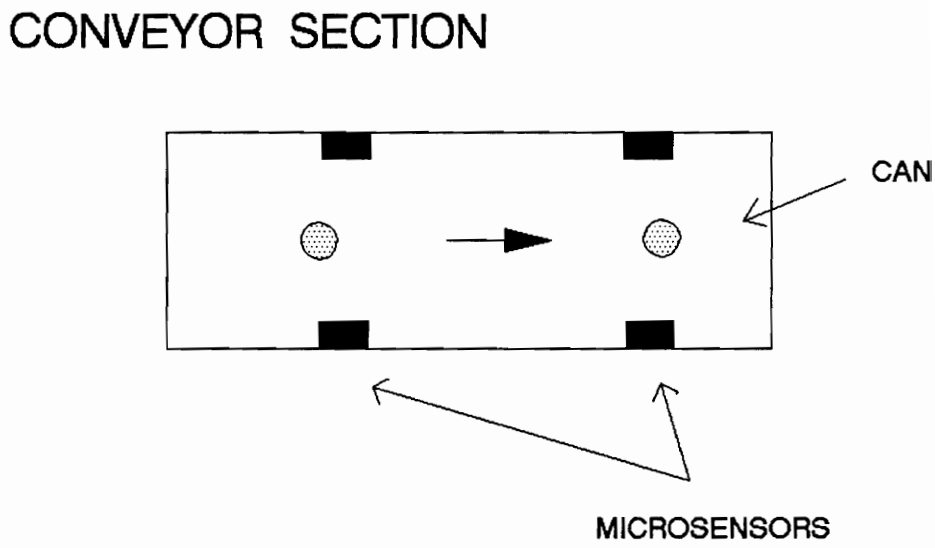

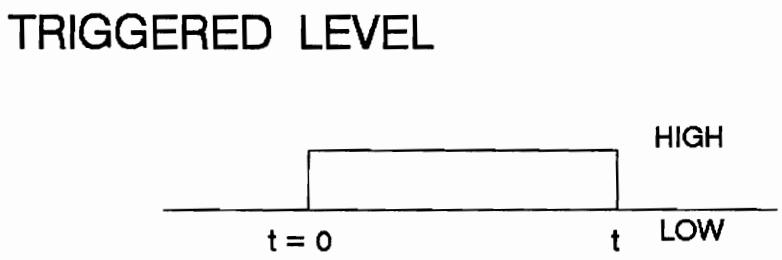

Figure 11 Time Measurements Method

CHAPTER 3

THEORETICAL DEVELOPMENT

The analyses of the forces that result from the air flow are very approximate models based on and verified by experimental results.

3.1 ANALYTICAL MODELS FOR LIFTING PRODUCTS

The lifting force, which must be at least equal to the product weight, is a function of the air supply pressure, the clearance between the conveying surface and the bottom of the product, and the hole shape and size.

Theoretical models will be developed in the case of the air flow from a straight circular hole.

3.1.1 ANALYSIS FOR THE LIFT OF PRODUCTS WITH CONCAVE BOTTOM SHAPE

Figure 12 shows the air flow conditions used in the analysis. The flow is assumed to be inviscid and

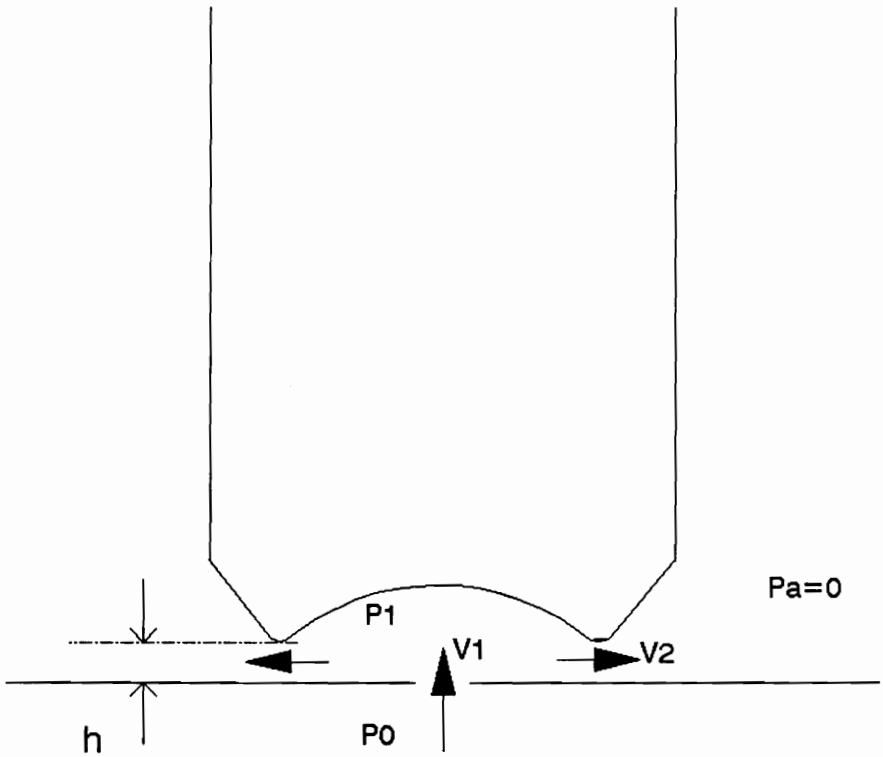

Figure 12 Air Flow Conditions Used in the Analysis for the Lift

incompressible. The essential assumption is to suppose a constant pressure P_1 inside the concavity of the product bottom. The supply pressure in the duct, P_0, is assumed to be constant, and the air issues from the opening with a speed V_1. The air escapes the concavity at a speed V_2.

Two independent equations characterizing the flow have been derived from Bernoulli's theorem:

$$P_0 - P_1 = \frac{1}{2}\rho V_1^2 \qquad (19)$$

and

$$P_1 - P_a = \frac{1}{2}\rho V_2^2 \quad , \qquad (20)$$

where P_a is the atmospheric pressure and ρ is the air density. Conservation of the volume flow rate requires that

$$C_{d_1} A_1 V_1 = C_{d_2} A_2 V_2 \quad , \qquad (21)$$

where C_{d1} and C_{d2} are discharge coefficients, respectively assumed equal to 0.6 and 0.9. A_1 is the hole opening area and A_2 the clearance area between the object bottom and the conveying surface. The quantities P_1 and V_1 are calculated from Eqs. 19 through 21 and substituted into the general formula (see Eq.22) for the lifting force, equal to the sum of the air momentum and the force due to the pressure difference between the duct and the underside of the product; that is,

$$F = (P_1 - P_a) A_c + \rho Q V_1 \quad , \qquad (22)$$

where A_c is the cross-sectional area of the bottom surface of

the product. Program 1 (Appendix 1), which solves for Eqs 19, 20, 21, 22, calculates the variation of the lifting force with the supply pressure for a given "floating height" and hole size. Figure 13 shows a set of curves proposed for use to determine the pressure required to lift a certain mass at a given height above the track.

3.1.2 ANALYSIS FOR THE LIFT OF PRODUCTS WITH FLAT BOTTOM SHAPE

The analysis is the same as the gas bearing theory of Powell (1970). The flow is laminar between both parallel flat surfaces. Inertia forces due to the acceleration will be neglected compared with frictional forces due to viscous shearing; pressure is constant over any section normal to the direction of the flow; there is no slip at the boundaries between the fluid and the plate. In the actual flow, separation would be expected (See Fig 14); but, this is not included in the model. Applying these conditions to the Navier-Stockes equations, these results

$$\frac{\delta^2 u}{\delta z^2} = \frac{1}{\mu}\frac{\delta P}{\delta r} \quad . \tag{23}$$

Integrating twice and applying the boundary conditions u=0 at z=0 and z=h yields

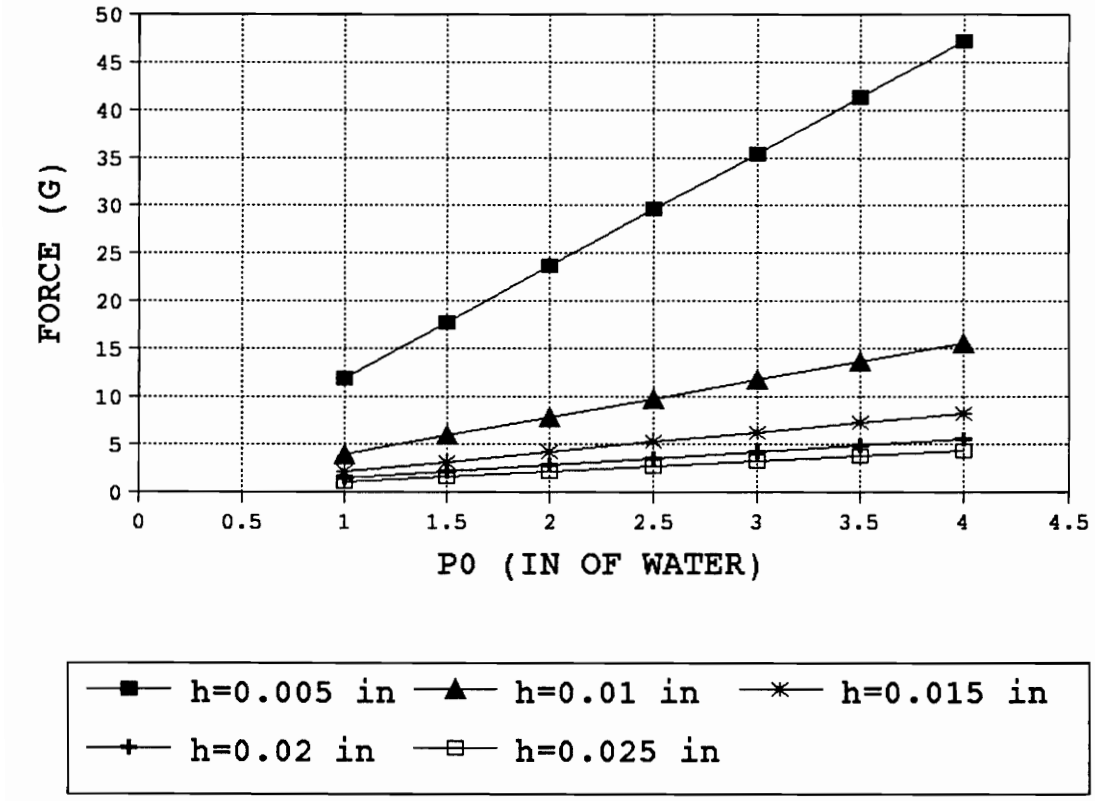

Figure 13 Theoretical Results for the Lift of Concave-Bottom Products

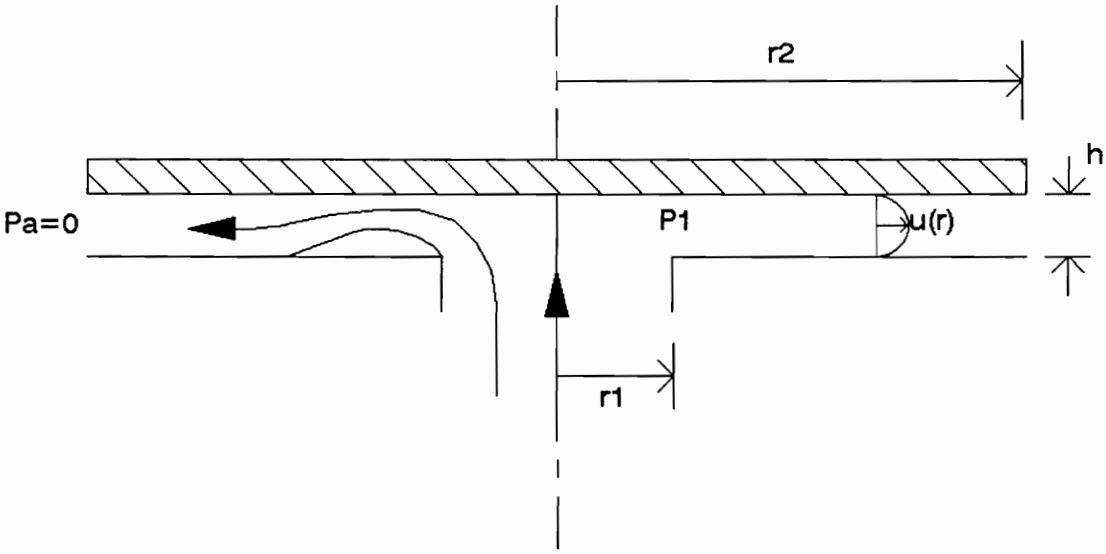

Figure 14 Flow Between Parallel Surfaces

$$u=\frac{1}{2\mu}\frac{dP}{dr}z(z-h) \quad . \tag{24}$$

Then the volume flow through annulus of width h and radius r is given by

$$q=2\pi r\int_0^h u\,dz \quad . \tag{25}$$

Substituting for u from Eq. 24 and integrating gives

$$\frac{dP}{dr}=-\frac{6\mu q}{\pi r h^3} \quad . \tag{26}$$

Integrating from $r=r_1$ to r yields

$$P(r)=P_1-\frac{6\mu q}{\pi h^3}\ln\frac{r}{r_1} \quad , \tag{27}$$

where

$$P_1=P_0-\frac{1}{2}\rho\left(\frac{q}{2\pi r_1 h}\right)^2 \quad . \tag{28}$$

Using the condition that $P(r_2)=0$ at $r=r_2$ allows a solution for q, function of r_2 and h. Finally, the lifting force F_z is calculated as

$$F_Z=P_0\pi r_1^2+\int_{r_1}^{r_2}P(r)\,2\pi r\,dr. \tag{29}$$

Program 2 (Appendix 2) calculates the lifting force as a function of the clearance for a given supply pressure and hole size. A set of curves is shown in Fig. 15 which represents the lift for various disc diameters.

This flow model does not give any negative value for

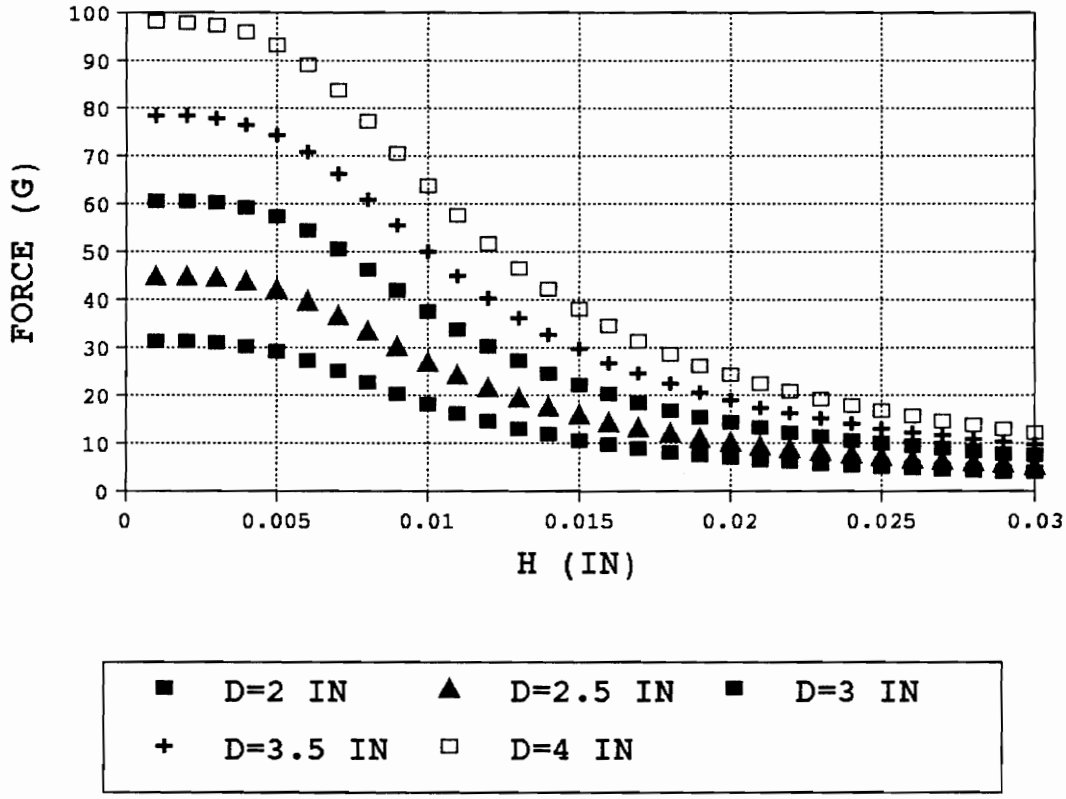

Figure 15 Theoretical Results for the Lift of Flat-Bottom Products

F_z whereas the tests do. However, adding the momentum effects to the viscous effects, did not improve the comparison with the experimental results; this is probably due to the flow separation.

3.2 ANALYTICAL MODEL FOR THE MOTION OF PRODUCTS

A simple model is developed, partially based on experimental data , that involves simple equations of fluid dynamics. The problem is limited to the can motion, in the x-direction, over one row of louvers and one of vertical jets. The purpose is to calculate the can speed along the conveyor. It is obtained by integrating

$$\frac{dV_{CAN}}{dt} = \frac{1}{m} F_T \quad , \tag{30}$$

where m is the mass of the can, F_T is the total force created by the fluid flow, and V_{CAN} is the can speed. Program 4 (Appendix 4) solves for the can speed using Eqs 30 through 34.

The total force, F_T, applied on the can will be the sum of the jet forces, F_{jets}, minus the drag force, Dg, depending on both velocity of the can and air velocity above the deck plate; i.e,

$$F_T = F_{jets} - Dg \quad . \tag{31}$$

The force due to the air jets, F_{jets}, is tangential to the direction of motion and is calculated from experimental results. In fact, experimental measurements of stationary force, F_x, applied on the static can can be used to calculate F_{jets} as

$$F_{jets} = \left(\frac{V_{jet} - V_{can}}{V_{jet}}\right) \sum_{i}^{N} F_{x_i} \quad , \tag{32}$$

where V_{jet} is the velocity of the jet, V_{can} is the speed of the can, and N is the number of jets with forces acting on the can. V_{jet} is calculated from the pressure distribution in the duct, measured experimentally,

$$V_{jets} = \sqrt{\frac{2 * P_0}{\rho}} \quad . \tag{33}$$

The air flux above the perforated plate also creates a force in the moving direction. Then, the drag force will be negative when the air velocity is greater than the can speed. The drag force is expressed as

$$Dg = \pm C_d \frac{1}{2} \rho \, (V_{CAN} - V_{AIR})^2 h^* d \quad , \tag{34}$$

where h^* is the height and d the width of the conveyed product. The profile of the air speed above the deck plate, V_{air}, is computed by Program 3 (Appendix 3), using the model, that refers to the control volume shown in Fig 16. The sum of

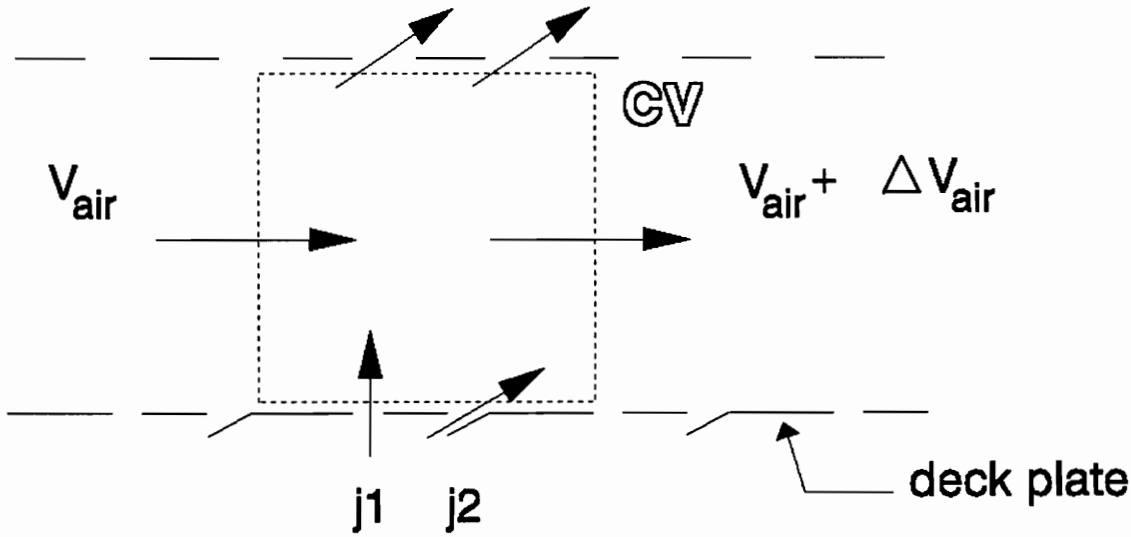

Figure 16 Control Volume Used in the Freestream Velocity Model

the forces generated by the air flow should be equal to the change of air momentum in a small volume (2 in. x 2 in. x 5 in.) above the deck plate containing one louver and one straight hole . The program solves for ΔV_{air} from

$$-\tau_W b\Delta x-\Sigma F_{CAN}=\rho bh_v V_{AIR}2\Delta V_{AIR}-\dot{m}_{j_1}V_{j_{x1}}+(\dot{m}_{j_1}+\dot{m}_{j_2}-\rho bh_v\Delta V_{AIR})V_{AIR} \quad , \tag{35}$$

where Δx, b, and h_v are, respectively, the length, the depth, and the height of the small volume , τ_w is the shear stress on the wall, V_{j1} is the inclined-jet speed, and m_{j1} and m_{j2} are the mass flow issuing from the slanted orifice and the straight hole. The quantity τ_w is calculated from

$$\tau_W=\frac{1}{2}C_f\rho V_{AIR}^2 \quad , \tag{36}$$

where C_f is the friction coefficient (assumed to be 0.003-0.005). Both mass flow are calculated from

$$\dot{m}_j=C_d A_j \rho V_j \quad , \tag{37}$$

where C_d is assumed to be 0.65 for sharped-edges holes, A_j is the section area of the hole, and V_j is the jet velocity.

CHAPTER 4

RESULTS AND DISCUSSION

4.1 CALIBRATION RESULTS

The gage arrangement measures the strain in the beam due to the vertical force and the torque due to the fluid flow. As described in Section 2.1.2, both can be measured separately by wiring the strain gages differently. Thus, a correlation between the output voltage and the vertical force as well as one between the output voltage and the torque are required.

As expected, the response of the strain gages is linear, so a linear regression model for the data was performed.

4.1.1 CALIBRATION FOR THE VERTICAL FORCE

Figure 17 shows the excepted linear response of the strain gages. A linear regression is used to relate the voltage displayed by the instrumentation, ΔE_{out},and the vertical force applied on the beam, F_z in gram-force:

-a-

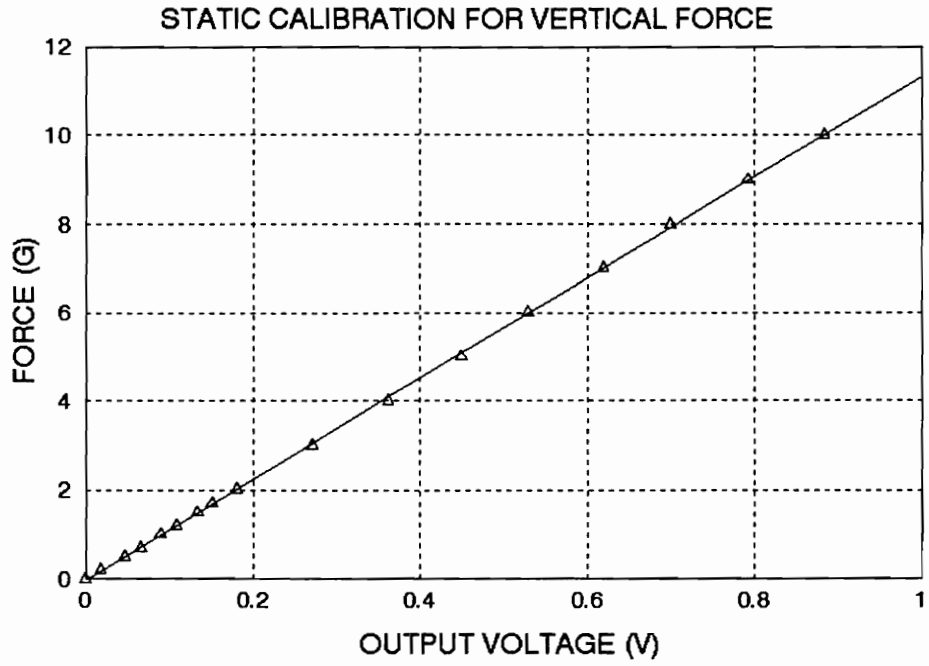

-b-

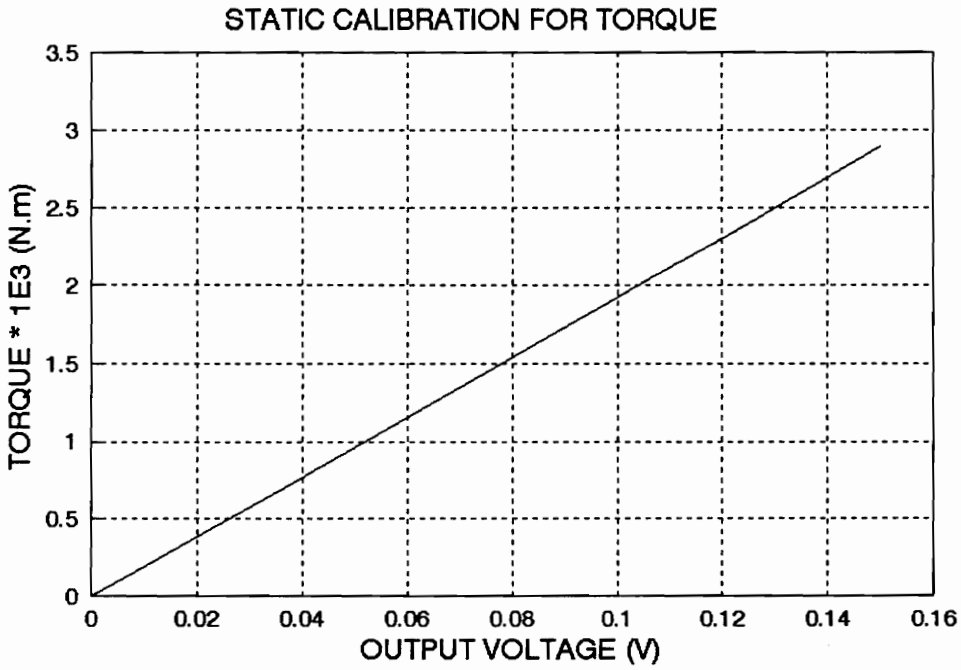

Figure 17 Calibration Results: a- Vertical Force
b- Torque

$$F_Z = 11.3\ \Delta E_{OUT}\ , \tag{38}$$

The coefficient of regression is equal to 0.9998.

4.1.2 CALIBRATION FOR THE TORQUE

An appropriate calibration with weights permits relating the output voltage and the amplitude of the force applied parallel to the beam:

$$\Delta E_{OUT} = 0.0259\ F\ , \tag{39}$$

where F could be F_x or F_y depending on what force is to be measured. The coefficient of regression is equal to 0.9997.

One must remember that this correlation is dependent on the length of the rod used for the calibration. The length of the rod was 2 in.. Thus, for any length L (in meters) from the point where F is applied to the center of the beam, the correlation is

$$\Delta E_{OUT} = \frac{0.0259}{2*2.54e\text{-}2}\ L\ F \tag{40}$$

The regression used to correlate the torque, corresponding to the force, with the output voltage of the circuit is independent of the length of the rod. Using Eq. 40 for the expression of F, and the definition of the torque, the relation between the torque and the output voltage is

$$T=F.L=0.01924\ \Delta E_{OUT}\ , \qquad (41)$$

where T, the torque, is in N.m.

4.2 JET IMPINGEMENT FORCES

The objects being transported on a conveyor track float on a cushion of air. The amplitude of the forces due to the air flow depends on many parameters, such as the air supply pressure, hole patterns, shape,size, etc.. It is simple to predict the effects of a change of pressure on the lifting force since the lifting force is proportional to the supply pressure. However, the influence of other parameters is not obvious.

The study is focused on the measurement of forces as a function of the shape of holes, classified into two categories, straight circular holes and slanted openings. The experimental setup was built such that plates with different single holes are interchangeable.

4.2.1 AIR FLOW THROUGH A CIRCULAR OPENING

A relatively small circular opening with a diameter of 0.1719 in. (4.37 mm) has been used for the tests. For all

the experiments, the air supply pressure is fixed at 3 in. of water (747 Pa). The force due to the vertical air jet supports the product and depends on the shape of the supporting surface of the object. A can with an original concave bottom and a can on which a thin disc has been fixed are tested.

4.2.1.1 LIFTING FORCES ON A CONCAVE-BOTTOM PRODUCT

To check the validity of the tests, three experiments are conducted with the same conditions of pressure. The air supply box is placed under the can so that the air jet is impinging in the center of the can bottom. Figure 18 shows that the repeatability of the results is acceptable. However, when the gap between the bottom of the can and the hole is less than 0.01 in. (0.25 mm), one notes a deviation between data points and the average curve, which is due to the drift of the gages, and a possible error in the "zero-clearance" determination. In fact, a slightly-different "zero" gap hand-set at the beginning of each experiment causes a discrepancy of a few grams for the amplitude of the lifting force. For very small gaps, a difference of 0.001 in. (0.025 mm) of one of the three micrometers creates a decrease in lifting force of 0.7 gram-force (6.9×10^{-3} N).

For small clearances of 0.001 to 0.008 in. (0.025 to 0.2 mm), the lifting force decreases strongly with an increase

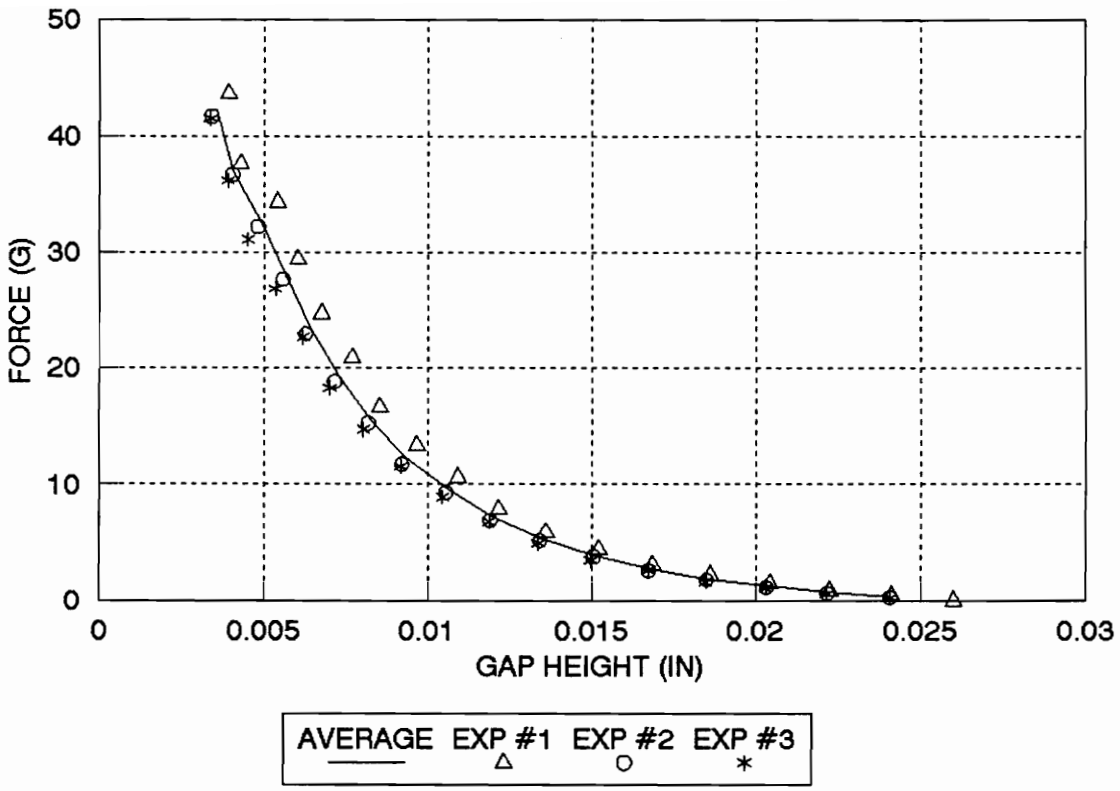

AIR JET IMPINGEMENT AT THE CAN CENTER
HOLE DIAMETER = 0.1719 IN
P = 3 IN OF WATER

Figure 18 Repeatability of Tests

of clearance. Then, the curve approaches zero lift more gradually.

Figure 18 could be used to determine the floating height of products of different weights when the pressure is 3 in. of water (747 Pa) and the diameter of the air supply hole is 0.1719 in. (4.37 mm). For instance, the thickness of the air cushion to support a 12-gram aluminum can should be in the order of 0.009 in. (0.23 mm).

To convey products correctly with no problems, the layer of air must be higher than the irregularities of the track surface and the products.

Figure 19 shows the comparison between the theoretical and experimental results. The curve representing the theoretical model, developed in Section 3, fits quite well with the experiments except when the layer of air between the object and the conveying surface is greater than 0.015 inch (0.38 mm). In fact, the model does not predict a negative force that has been detected experimentally for larger clearances.

The previous experiments are conducted with the vertical jet positioned right below the center of the can. Then, to examine eventual changes due to a jet, not impinging in the center of the can bottom, an experiment is conducted.

The lifting force, which is due to a building

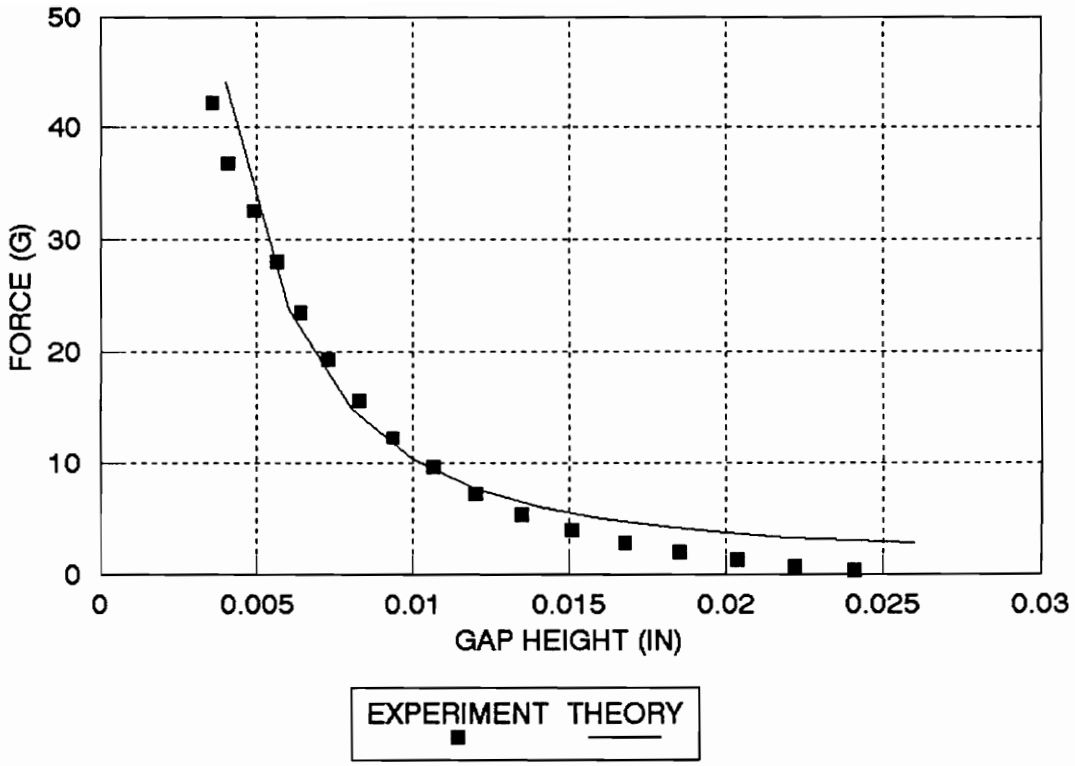

Figure 19 Theoretical and Experimental Results for the Lifting Force

pressure inside the concave bottom, is measured as the hole is located at various radii from the center of the can and fixed at a constant height. To plot Fig. 20, we assume that the clearance, increased a bit by the deflection of the beam, stays constant during the experiment. This assumption is valid because the lifting force appears to be almost constant whatever the hole position; so, the deflection, proportional to the force, is also constant.

These results prove that the distribution of pressure is uniform in the concavity of the can bottom. It confirms the assumption made in the model to describe the flow under a concave bottom product (See Section 3.1.1).

The lifting force drops to zero as the can passes the air supply hole.

4.2.1.2 LIFTING FORCES ON A FLAT-BOTTOM PRODUCT

Flat discs of different diameters (2 in. (5 cm) - 2.5 in. (6.3 cm) - 3 in. (7.5 cm) - 4 in. (10 cm)) were fixed to the bottom of the can. The 0.1719 in. (4.37 mm) diameter hole was set below the center of the disc and the pressure is set at 3 in. of water (747 Pa). Three experiments are conducted to check the repeatability of the tests, and to obtain an average curve for each of the discs.

As expected, the lifting force per unit area

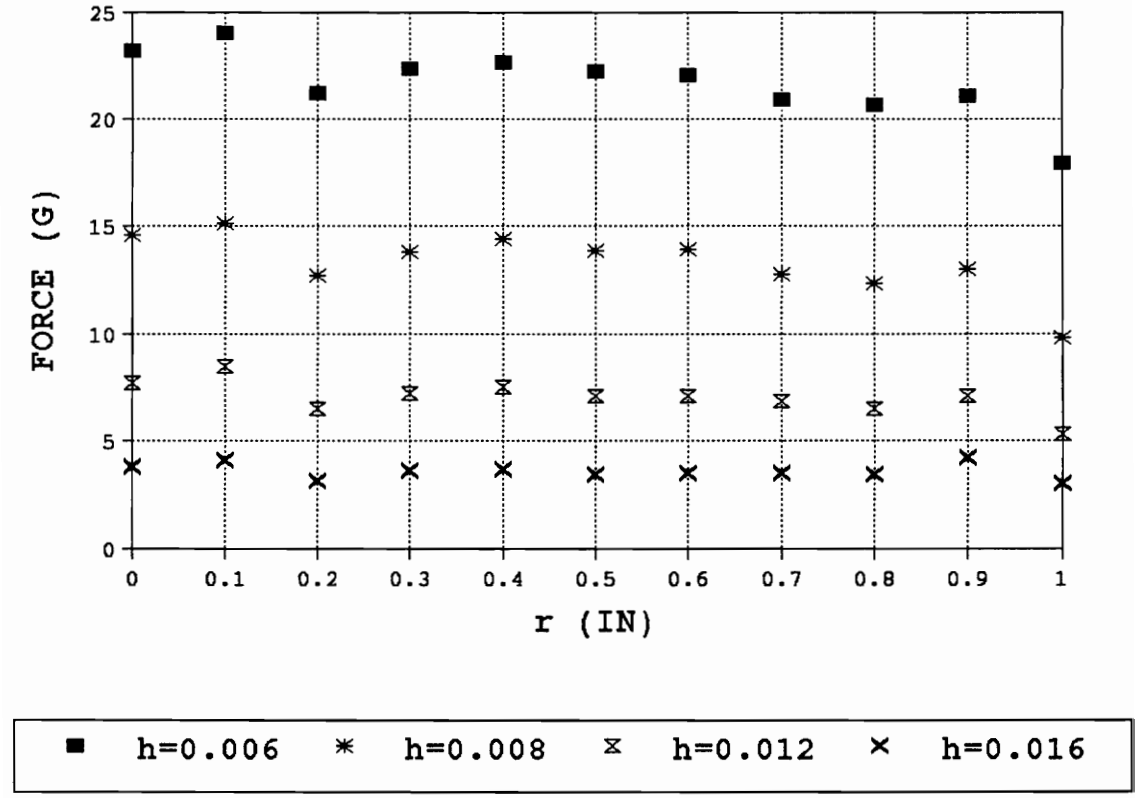

Figure 20 Variation of the Lifting Force in the r-Direction

decreases with an increase of the gap height. Experiments show that negative forces appear for a clearance between 0.02 in. (0.5 mm) and 0.3 in. (7.5 mm). Only positive forces are displayed.

Figure 21.a shows the average curves obtained for various disc diameters. Obviously, the floating height of any product, having a given weight, increases with its base area. Figure 21.b shows the lifting force per unit area as a function of the clearance, that is almost constant from 0.01 to 0.02 in. (0.25 to 0.5 mm).

A comparison between experimental data and computed data (See Appendix 2), is shown in Fig. 22. Even if the trend of curves is similar in both cases, the analysis does not predict negative forces.

It is interesting to compare the lifting force on the can with its original concave bottom of 2 in. in diameter and the can arranged with a flat disc of the same size (See Fig. 23). According to the results, 12-gram empty aluminum cans with a flat bottom would be supported nearly at the same height as cans with an original concave bottom.

But, we do not know how they would be conveyed along the conveyor. Information about the directional force due to slanted openings is required.

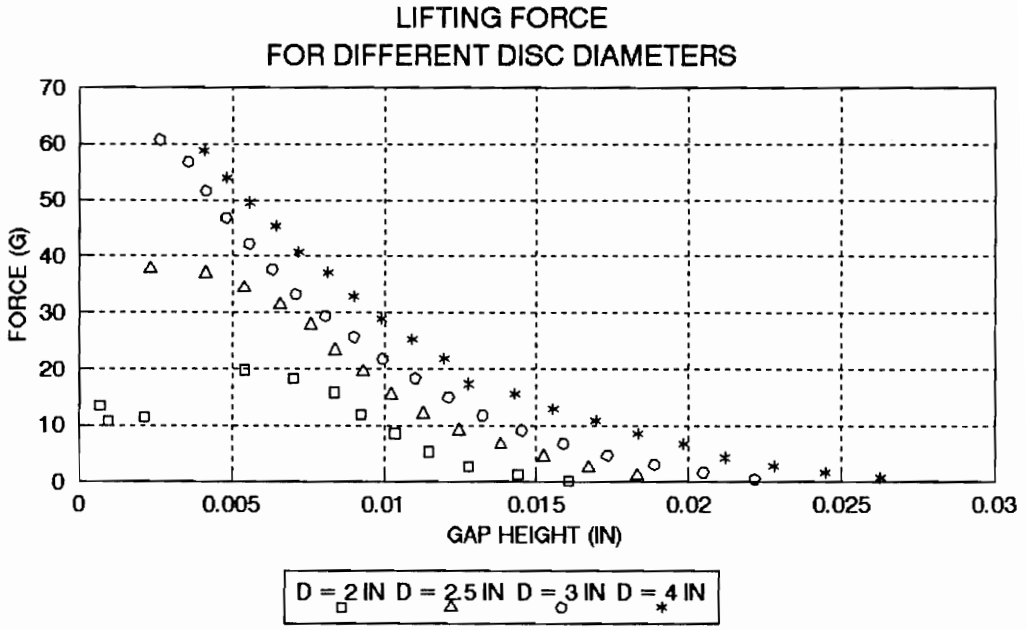

AIR JET CENTERED UNDER THE DISC
HOLE DIAMETER = 0.1719 IN
P = 3 IN OF WATER

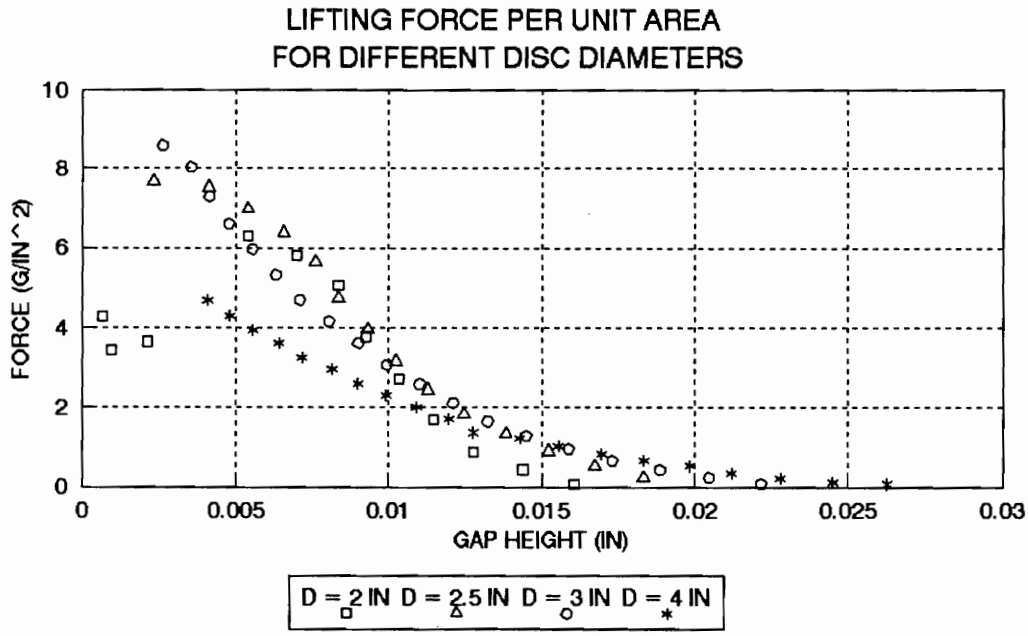

Figure 21 Comparison of the Lifting Force for Different Disc Sizes

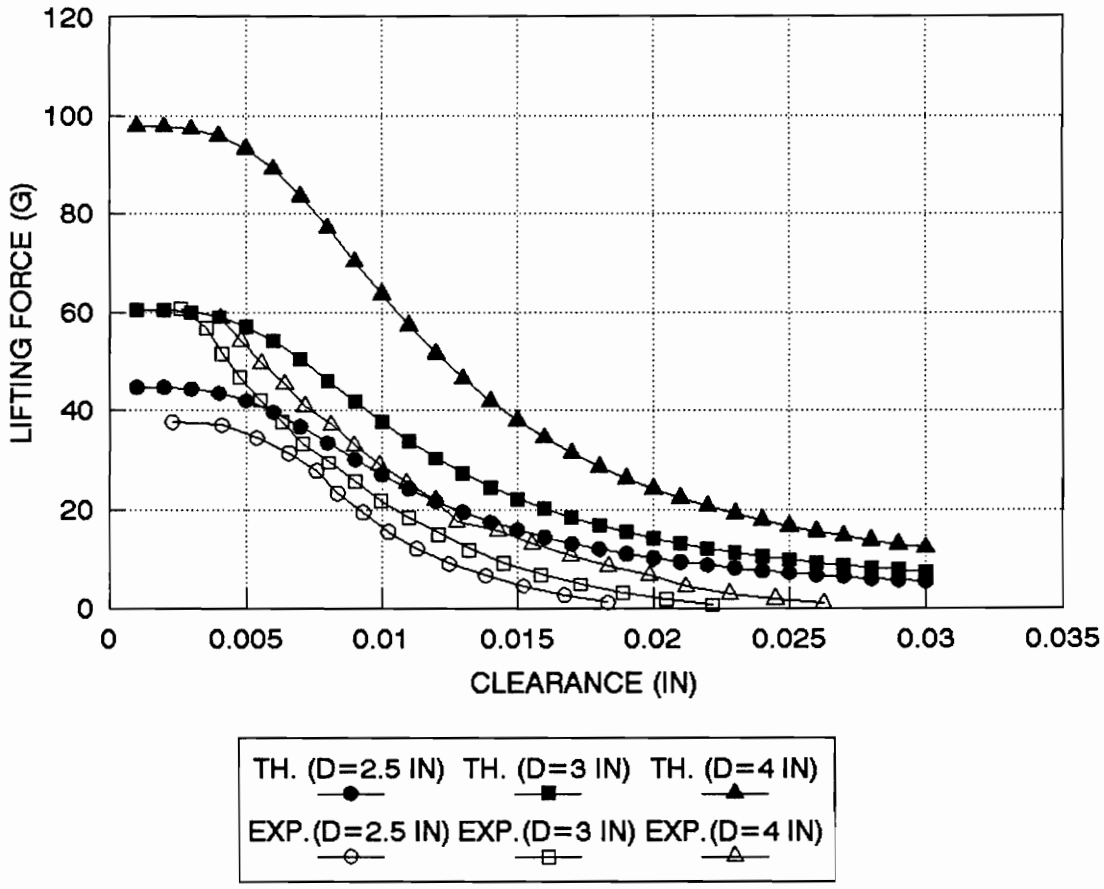

Figure 22 Theoretical and Experimental Data for the Lifting Force Applied on Discs

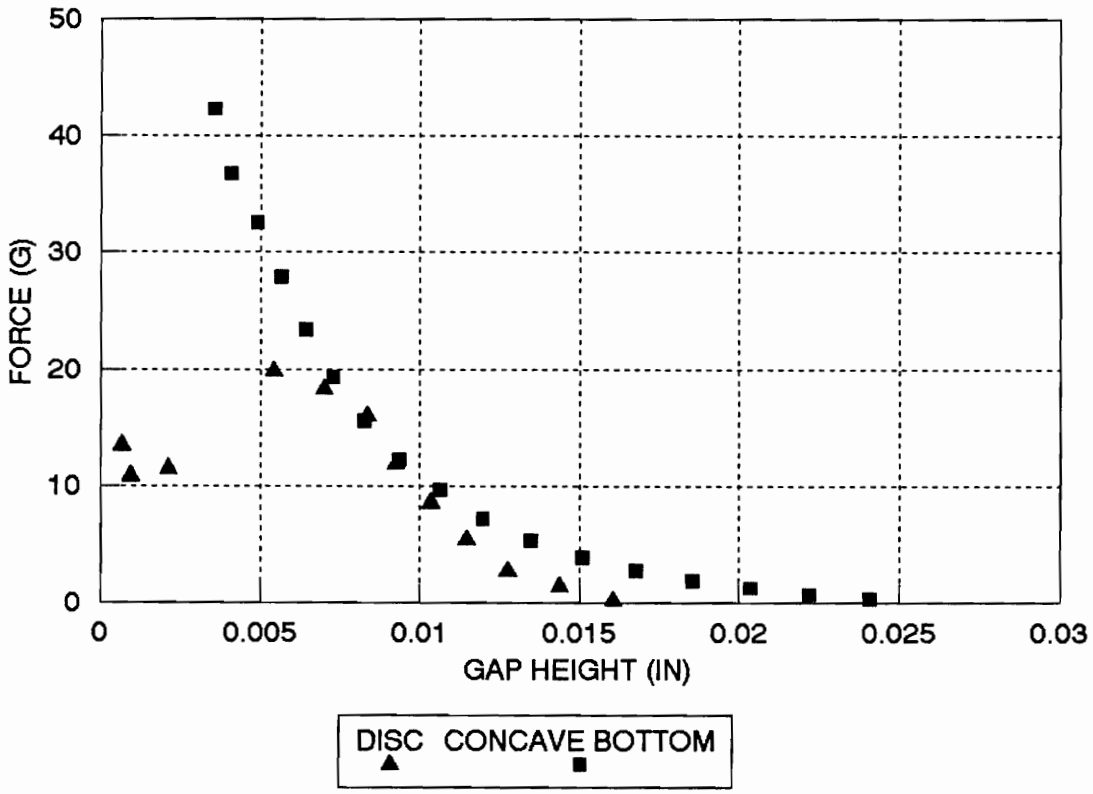

Figure 23 Comparison Between the Force Applied on a Concave Bottom and That Applied on a Flat Bottom of the Same Size.

4.2.2 AIR FLOW THROUGH A SLANTED OPENING

A slanted opening in the deck plate generates not only a moving force but also a lifting force.

To measure those forces, a single slot similar to the openings of the actual deck plate of the conveyor designed by *Simplimatic Engineering Co.* is tested on a concave bottom product.

4.2.2.1 LIFT GENERATED BY THE AIR FLOW

The air flow coming through the slanted hole is not globally characterized by only one component in the direction of motion. In fact, the lifting force created by the flow field appears to be at least ten times as large as the tangential force.

The amplitude of the lifting forces due to the flow issuing from straight holes and slanted holes is shown in Fig. 24. The tested object is a concave-bottom can. The jet impingement is on the center of the can during the experiment.

It appears that the lifting force generated by the louver is of the same order of magnitude as that created by a vertical jet. That means that the straight hole is not necessarily required to generate a lifting force; thus, a conveyor deck grid designed only with this kind of tangential

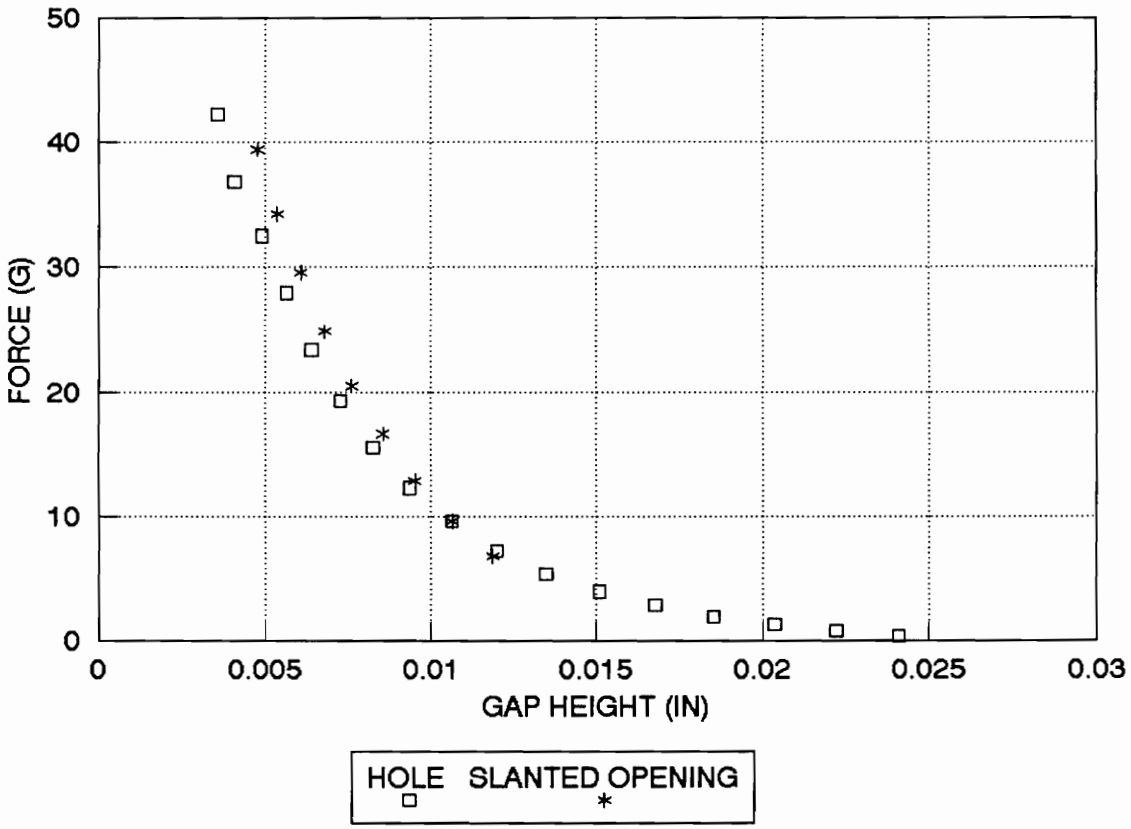

Figure 24 Comparison of the Lifting Force Applied on a Curved Bottom for Two Different Hole Shapes

holes could be conceived.

However, when the louver or "slanted" hole is moved away from the center of the can, the lifting force drops a great deal, whereas it does not for a straight hole. In fact, air escapes easily from the concavity since the jet is inclined.

Figure 25 show the lift amplitudes for different positions (Xc) of the center of the slanted hole under the can.

As the hole is located everywhere under the can centerline, corresponding to the direction of motion, the lift remains high even when the opening is three-quarters of the radius from the center of the concave bottom. However, when the hole is near the periphery, the lift drops.

4.2.2.2 MOVING FORCES

4.2.2.2.1 IN THE DIRECTION OF CONVEYANCE

The amplitude of the directional force is calculated from data corresponding to the moments due to F_x and F_z. However, the moment of F_z is assumed to be small compared to the moment of F_x because F_z, due to the building pressure in the concavity, is supposed to be aligned with the center of gravity of the can.

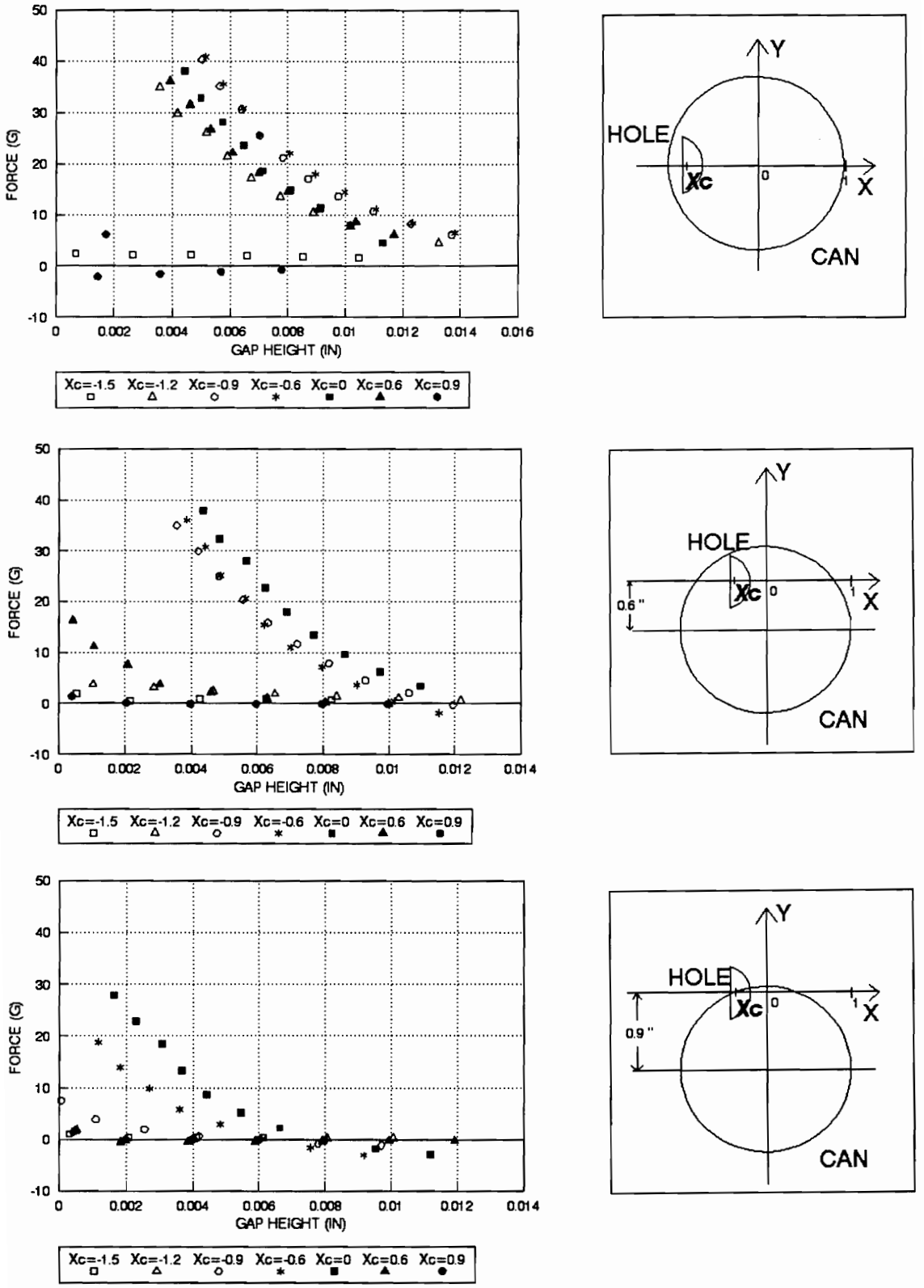

Figure 25 Lifting Force for Different Hole Positions

The moment of F_x is exactly measured when the center of the can is placed on the y axis (See Fig. 26). These data give an idea of the tilting effects in the direction of motion. Figure 26 shows the experimental results obtained when the hole is placed at different positions below the can. The maximum tangential force of 1.8 gram-force (0.0176 N) appears when the can is right above the hole. It does not drop to zero even when the can has just moved over the jet.

4.2.2.2.2 PERPENDICULAR TO THE DIRECTION OF CONVEYANCE

The quantity F_y (See Fig. 8) corresponds to the side force due to the flow issuing from the louver. It is evaluated from data corresponding to the moment of the force F_y and F_z. Figure 27 shows the results that denote effects of suction: a louver located on the right side of the can generates a force that attracts the can to the right. The amplitude of F_y is half that of F_x.

4.3 CAN MOTION ON THE ACTUAL CONVEYING SYSTEM

Empty standard-shape aluminum cans are tested on an actual conveyor to measure the speed of motion. Two series of tests are done on a ten-feet long module , first closed at both ends ,and finally coupled with another 10-feet (3 m)

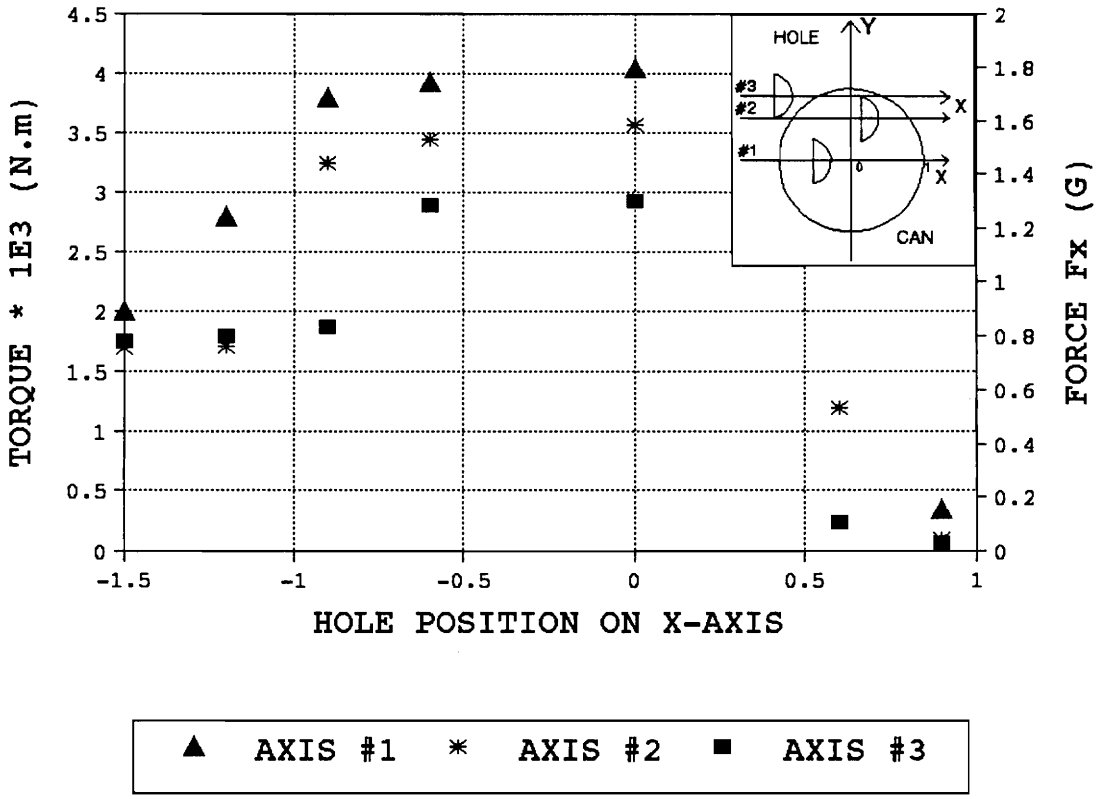

Figure 26 Torque due to F_x and F_z at Different Jet Positions

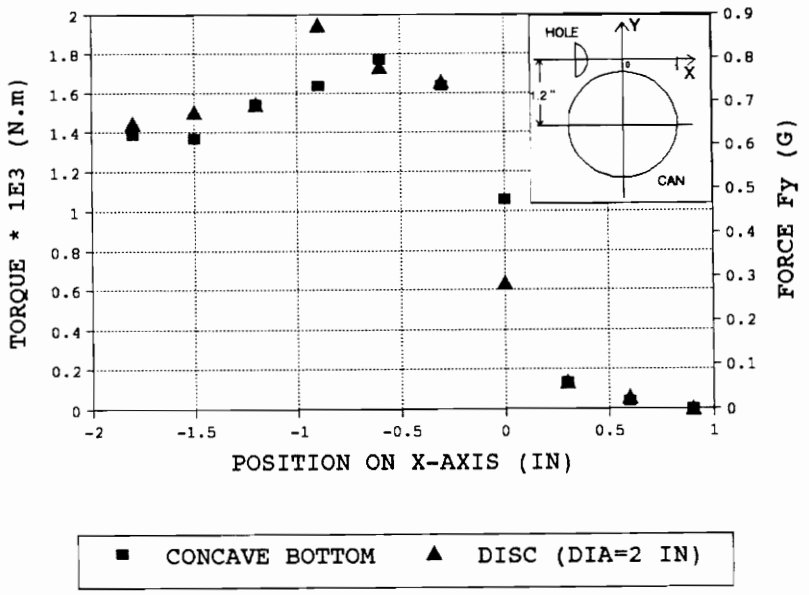

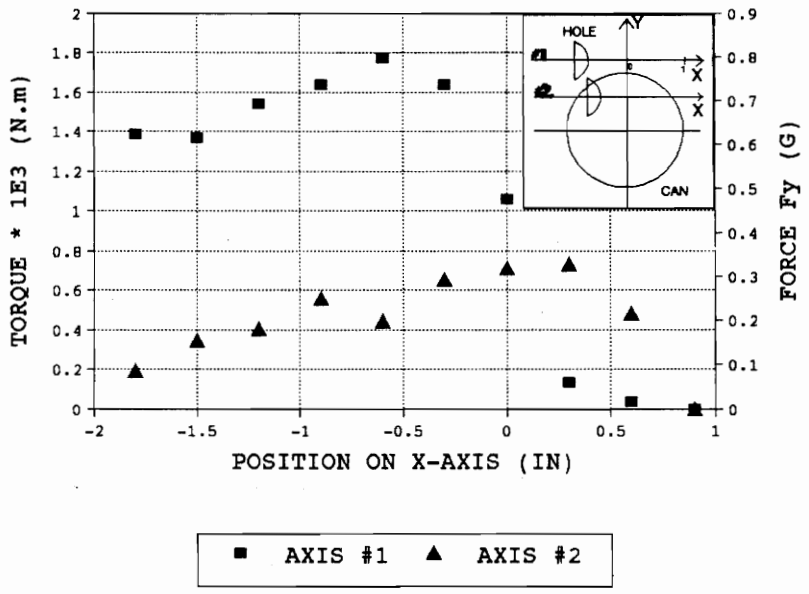

Figure 27 Torque due to F_z and F_y:
-a- for Different Shape Bottoms
-b- at Different Jet Position under a Concave Bottom

long module with the same air supply.

4.3.1 EXPERIMENTAL RESULTS

The can is positioned manually at the entrance of the track. Each can is evidently not released exactly with the same force and at the same position. So, each can behavior may be slightly different. For example, a can positioned above a row of slanted jets moves most of the time above this row, without spinning. In the other cases, the can deviates to the closest row of slanted holes and moves straight. Tilting effects are observed as well as spinning effects occasionally. Since the motion is somewhat different for all the cans, an average of about thirty time-measurements is required for each position of the microsensors on the conveyor. The standard deviation is around 0.06 second for all the series of measurements.

A fitting polynomial correlates the distance covered by the can and the time measurements. The derivative of this polynomial is considered to be the can speed. Since a second degree polynomial fits the data quite well, the speed is a first degree polynomial, and its derivative gives an idea of the acceleration which is constant.

First, only one section of conveyor is tested; then, another section with no additional centrifugal fan is coupled perpendicularly to the other. The distribution of pressure in

the duct for both cases is shown in Fig. 28. When the two sections are coupled, the pressure drops to a mean value, that is 40 percent less than the pressure in only one section. However, Fig. 29 shows that the can speed decreases only by 20 percent.

The can acceleration in one 10-feet (3 m) long section is about 14 ft/s^2 (4.3 m/s^2), whereas it is 11 ft/s^2 (3.3 m/s^2) when the two sections are coupled.

4.3.2 THEORETICAL RESULTS

After computing the air velocity above the deck plate, the can speed is calculated from the analysis done in Section 3.2. A comparison between the expected speed and the tests results is shown in Fig. 30.

The model is close to the reality in the first part of the conveyor section; then, the analysis predicts a can speed greater than the actual speed. The fact is that, the friction effects of the can on the top grid could not be modeled and it would have reduced the theoretical speed.

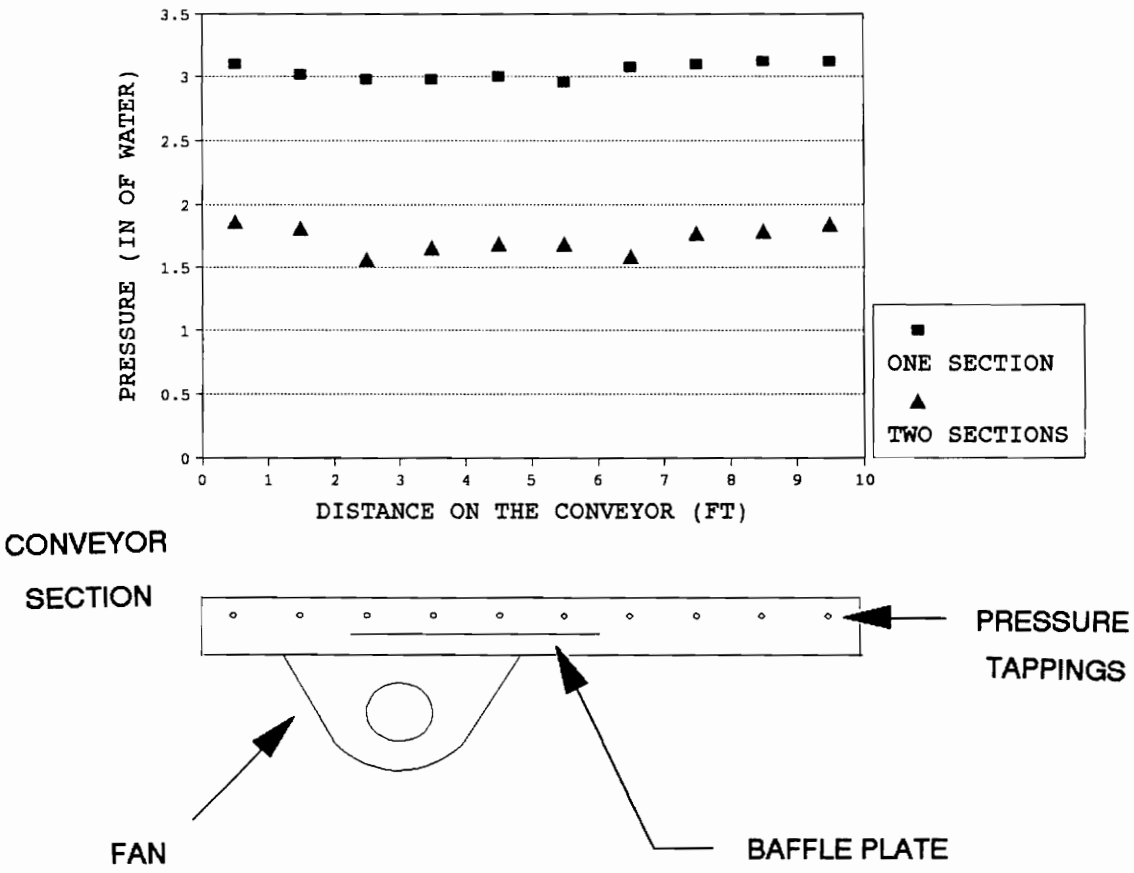

Figure 28 Distribution of Pressure in the Duct

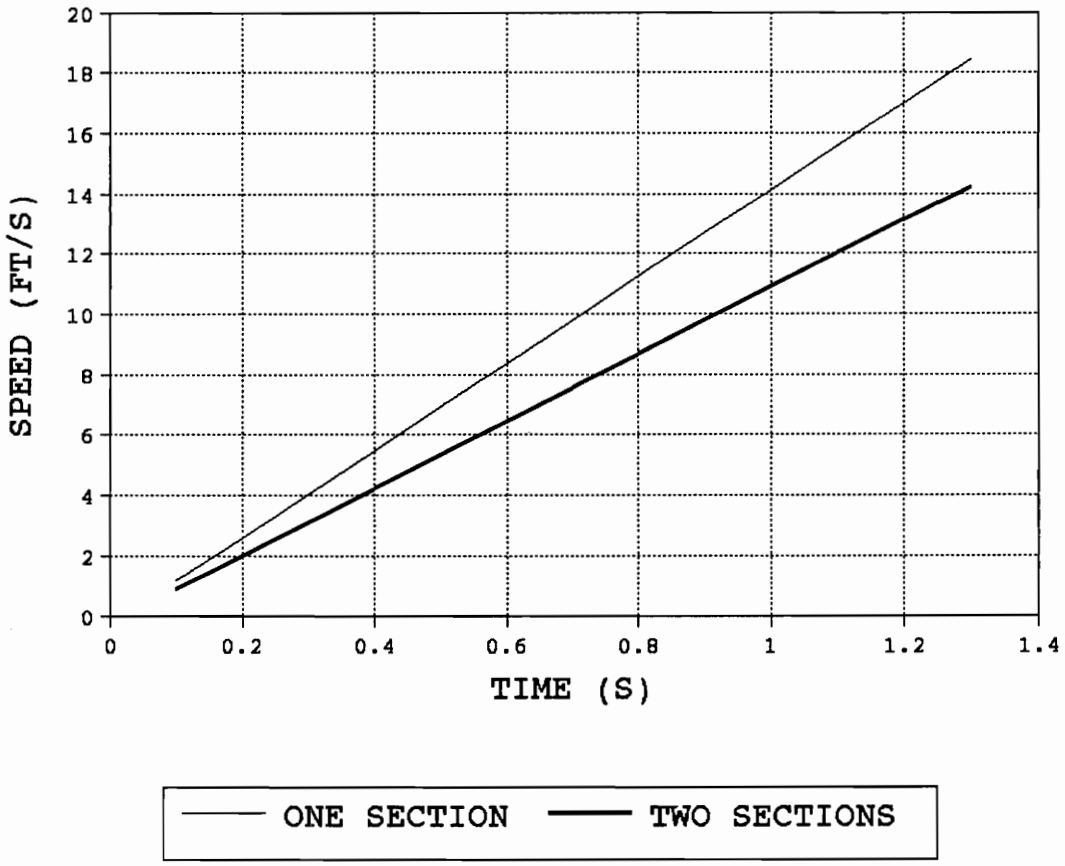

Figure 29 Speed Measurements

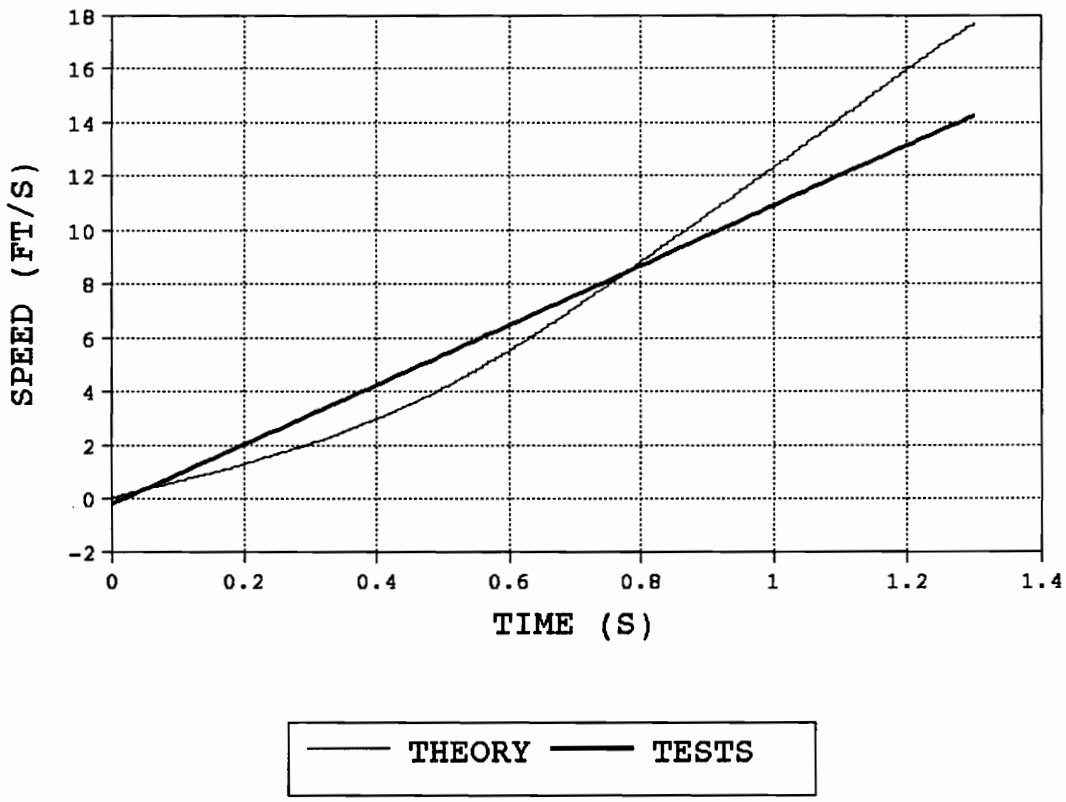

Figure 30 Theoretical and Experimental Can Speed

CHAPTER 5

CONCLUSIONS AND RECOMMENDATIONS

As far as the experimental work is concerned, the method of using an arrangement of strain gages to detect small forces is very satisfactory. The results are repeatable; the deviation between measured and actual forces is about 4 percent. In fact, the sources of experimental errors come from the inaccuracy of the "zero-clearance" at the beginning of experiments, the drift of semi-conductor gages due to self-heating, and the supply pressure reading inexactness.

The results show that a slanted hole generates also a lifting force equivalent to the lift due to a straight hole when the can bottom center is above the jet opening. The results for either hole can be used to determine the pressure required to lift an article of a certain mass at a given height, or knowing the pressure, determine the "floating height" of the article. For instance, a 12-gram aluminum can floats at an height approximately equal to 0.009 in. (0.225 mm) above the deck plate when the supply pressure is about 3 in. of water (747 Pa).

The tangential force on a can is approximately 10 times as small as the lifting force due to the same hole. Actually, the lift is mostly due to an increased pressure inside the concavity of the can bottom, whereas the tangential force is related to the momentum of the jet.

When running the experiments with the conveyor, a large air flow above the deck plate has been noticed; its velocity is a primarily factor affecting the can speed.

The representation of the flow field can be very complicated because the conveyor design depends on a number of variables (hole size and pattern, product shape) with infinite combinations. We choose to develop analytical models specific to the transportation of cans and flat products; hole patterns were limited to a straight hole and a slanted opening.

A program computing the speed of cans is based on the characteristics of the conveyor used for the experiments. The variation of some parameters, such as the pressure, the hole size, the product weight, is possible. It could be useful for developing design procedures.

Future work using this research will be to reduce the data to a form that can be implemented in computer aided engineering for the design of future systems.

Finally, further testing of straight and tangential

forces should include the effects of various inclinations of slanted jets. Concerning additional tests with the actual conveyor, we would suggest testing different kinds of guide-plates covering the track section.

BIBLIOGRAPHY

CHANDRA, C. J. G., [1987], "Analysis of Air Film in Conveyor Pressurized by Two Parallel Slots: Effect of Titling of Package in Both Longitudinal and Transverse Directions", Communications in Applied Numerical Method, Vol. 3, pp.469-478, 1987.

CHANDRA C. J. G., [1990], "Investigation of Air Film Conveyor Pressurized Through Multiple Holes", Finite Elements in Analysis and Design, Vol. 6, pp.235-243, 1990.

DANLER R.W., [1981], "Air Conveyor For Bottles and Bottles Preforms", U.S. Patent Document 4,284,370, 1981.

FUTER, R. F., [1983], "Surface Flow Air Conveyor With Plenum Mounted Fan Wheel", U.S. Patent Document 4,392,760, 1983.

LENHART, R. A., [1983], "Air Conveyor", U.S. Patent Document 4,369,005, 1983.

LENHART, R. A., [1988], "Divergent Single Filer", U.S. Patent Document 4,730,955, 1988.

LINDSTROM, D. E., et al, [1987], "Air Conveyor", U.S. Patent Document 4,710,068, 1987.

Marks' Standard Handbook for Mechanical Engineers, [1978], New York, Mc Graw-Hill, 1978.

MORI H., YABE H. and OHNISHI, [1966], "Analysis of Externally Pressurized Rectangular Pads with Multiple Holes", ASLE Transactions, Vol. 9, pp.391-401, 1966.

MORI H., YABE H., [1971], "Theoretical Investigation of Externally Pressurized Air-Suspension Conveyer With Multiple Holes", Journal of Lubrication Technology, pp.279-286, April 1971.

POWELL, J. W., [1970], "Design of Aerostatic Bearings", pp.35-41, 1970.

SPILLMAN, J. J., [1985], "An Improved Form of Air-Bed Conveyor", Symposium on Air Cushion Handling , paper 6, 1985.

APPENDICES

PROGRAM 1

```
{ THIS PROGRAM CALCULATES THE LIFT Fz DUE TO A VERTICAL AIR JET }
{ APPLIED ON THE CONCAVE BOTTOM OF A CAN IN FUNCTION OF THE     }
{ SUPPLY PRESSURE P0 AND THE CLEARANCE h BETWEEN THE CAN BOTTOM }
{ AND THE DECK PLATE                                            }


program Model1;
uses printer;

type Text_file=text;

const
     d1=0.1719;      (*in*)              (* hole diameter *)
     d2=2;           (*in*)              (* can bottom diameter *)
     rho=0.076752;   (*lbm/ft^3*)        (* air specific weight *)
     Pa=0;

var
    f1:text_file;
    i,j:integer;
    p0,p1,v1,v2,fz:array [0..50] of real;
    Acan,A1,A2,h,P,cd1,cd2,k:real;

begin
    assign (f1,'varcds.dat');
    rewrite (f1);
    writeln('what is the value of Cd1 ?');
    readln (cd1);
    writeln ('what is the value of Cd2 ?');
    readln (cd2);
    h:=0;
    P:=0.50;  (*in water*)
    A1:=pi*d1*d1/4;          (*in^2*)
    Acan:=pi*d2*d2/4;        (*in^2*)
    write(lst,'       ');
    for j:=1 to 7
    do begin
            P:=P+0.5;
            write(lst,p:8:3);
            end;
    writeln(lst);
    write(lst,'       _____________________________________');
    writeln(lst,'_____________________________________');
    writeln(lst);
    for j:=1 to 30
    do begin
           h:=h+0.001;  (*in*)
           A2:=pi*d2*h; (*in^2*)
```

```
            k:=sqr(cd1*A1/(cd2*A2));
            write(lst,h:5:3,' ');
            p0[0]:=0.5;
            for i:=1 to 7
            do begin
                  P0[i]:=P0[i-1]+0.5;
                  P1[i]:=k/(k+1)*p0[i];
                  v1[i]:=sqrt(2*(P0[i]-P1[i])/rho*5.2*32.2);
                  v2[i]:=sqrt(2*(P1[i]-Pa)/rho*5.2*32.2);
                  Fz[i]:=((P1[i]-Pa)*Acan*5.2/144+rho*cd1*A1*sqr(v1[i])/
                        (144*32.2))/9.8*1e3/0.225;                    (*g*)
                  write(lst,fz[i]:8:3);
            end;
            writeln(f1,h:5:3,' ',fz[5]:8:3);
            writeln(lst);
         writeln;

      end;

writeln(lst);
close(f1);

end.
```

PROGRAM 2

```
{ THIS PROGRAM CALCULATES THE LIFT DUE TO A VERTICAL AIR JET    }
{ APPLIED ON A FLAT DISC IN FUNCTION OF THE RADIUS OF THE DISC }
{ AND THE CLEARANCE BETWEEN THE DISC AND THE DECK PLATE        }
{ THE PRESSURE IS FIXED TO 3 IN OF WATER BUT IT CAN BE CHANGED }


program modeldisc;
uses printer;

const
    nd=30;  {nb of data}
    r1=2.18313e-3;      (* m *)
    mu=1.82e-5;         (* kg/m/s *) (* at 20 C*)
    rho=1.2289;          (* kg/m^3 *)
    pi=3.1415927;
    p0=746.928;         (* Pa *)
    fac=2.54e-2;        (* m/in *)

type data=array[1..nd,1..nd] of real;
     name=string[5];
     vector=array[1..nd] of real;

var q1,r,r2,h:real;
    rr,HH:vector;
    rpp,pp,q0,FF:data;
    name_file:name;
    i,j:integer;
    F3:text;
    RPT,RT:string[20];

procedure Write_File(f1:name;nb:integer;HA:vector;QA,FA:data);
type Text_File=Text;
var
   ff1:Text_file;
   Choice:char;
   hT,QT,FT:string[20];
   t,l:integer;
begin
Assign(fF1,f1);
rewrite(fF1);
for t:=1 to nb do
    begin
    str(HA[t],HT);
    write(fF1,HT,' ');
    for l:=1 to 5 do
        begin
        str(QA[l,t],QT);
        str(FA[l,t],FT);
        write(fF1,QT,' ',FT,' ');
        end;
    writeln(fF1);
    end;
close(fF1);
end;

function q(h,r2:real):real;
var a,b,c,SD:real;
begin
      a:=rho/2/sqr(r1*2*pi*h*fac);
```

```
      b:=6*mu*ln(r2*fac/r1)/pi/(h*h*h*fac*fac*fac);
      c:=-p0;
      SD:=sqrt(b*b-4*a*c);
      q:=(-b+SD)/(2*a);
end;

function F(r2,q,h:real):real;
var w,x,y:real;
begin
w:=pi*p0*sqr(r1);
x:=-12*mu*q/(h*h*h*fac*fac*fac)*(sqr(r2*fac)/2*(ln(r2*fac/r1)-0.5)+sqr(r1)/4);
y:=2*pi*(p0-0.5*rho*sqr(q/(2*pi*r1*h*fac)))*(sqr(r2*fac)/2-sqr(r1)/2);
F:=(w+x+y)/9.81e-3;
end;

function P(r,q,h:real):real;
var z:real;
begin
z:=p0-6*mu*q/pi/(h*h*h*fac*fac*fac)*ln(r*fac/r1);
p:=z-rho/2*sqr(q/(2*pi*h*fac*r1));
end;



{                  main prog              }
begin
r2:=0.75;
for i:=1 to 5   do
    begin
    r2:=r2+0.25;
    h:=0.0;
    for j:=1 to 30  do
        begin
        h:=h+0.001;
        q0[i,j]:=q(h,r2);
        HH[j]:=h;
        FF[i,j]:=F(r2,q0[i,j],h);
        end;
    end;
write('Enter the name of the file:');
readln(name_file);
Write_File(name_file,nd,HH,q0,FF);


r2:=1.5;
h:=0;
for j:=1 to 6 do
begin
     h:=h+0.002;
     q1:=q(h,r2);
     r:=0.0;
     for i:=1 to 10 do
         begin
         r:=r+0.02;
         pp[j,i]:=p(r,q1,h);
         rpp[j,i]:=pp[j,i]/746.93;
         rr[i]:=r/1.5;
         end;
      for i:=11 to 23 do
```

```
      begin
      r:=r+0.1;
      pp[j,i]:=p(r,q1,h);
      rpp[j,i]:=pp[j,i]/746.93;
      rr[i]:=r/1.5;
      end;
end;


assign(f3,'c:\pascal\presdisc.dat');
rewrite(f3);
for i:=1 to 23 do
    begin
    write(rr[i]:3:2);
    write(' ');
    str(rr[i]:3:2,RT);
    write(f3,RT,' ');
    for j:=1 to 6 do
        begin
        write (rpp[j,i]:7:7);
        write(' ');
        str(rpp[j,i]:6:5,RPT);
        write (f3,RPT,' ');
        end;
    writeln;
    writeln(f3);
    end;
close (f3);
end.
```

PROGRAM 3

```
{ THIS PROGRAM CALCULATES THE AIR VELOCITY ABOVE THE DECK PLATE  }

program V_track;
const
Cf=0.003;     (*friction coefficient*)
b=2;          (*width in*)
h=5;          (*height between the deck plate and the hold-down plate*)
dx=2;         (*increment length*)
rho=0.07672; (*air specific weight*)
Ajet1=0.0276;(*in^2 slanted jet*)
Ajet2=0.021; (*in^2 straight hole*)
Cd=0.65;
L=10;         (*length of conveyor*)
s=2;          (*spacing between two holes*)


var
i,j,N:integer;
{P0,Vjet:real;}
x,first,second,dV,V:array [0..1000] of real;
f1:text;

function Vjet(x:real):real;          { Vjet is calculated from }
var                                  { the pressure distribution profile }
P0:real;
begin
if ( (x>=0) and (x<0.5) )
   then P0:=-0.06*x+1.95 else
if ( (x>=0.5) and (x<1.5) )
   then P0:=-0.1*x+1.97 else
if ( (x>=1.5) and (x<2.5) )
   then P0:=-0.24*x+2.18 else
if ( (x>=2.5) and (x<3.5) )
   then P0:=0.1*x+1.33 else
if ( (x>=3.5) and (x<4.5) )
   then P0:=1.68 else
if ( (x>=4.5) and (x<5.5) )
   then P0:=0.02*x+1.59 else
if ( (x>=5.5) and (x<6.5) )
   then P0:=-0.03*x+1.865 else
if ( (x>=6.5) and (x<7.5) )
   then P0:=0.11*x+0.955 else
if ( (x>=7.5) and (x<8.5) )
   then P0:=0.02*x+1.63 else
if ( (x>=8.5) and (x<=10) )
   then P0:=0.04*x+1.46;


Vjet:=sqrt(2*5.2*32.2/rho*P0);
end;


begin
N:=trunc(L/(s/12));
x[0]:=0;
v[0]:=5;
     for i:=0 to 100 do
            begin
```

```
            first[i]:=-Cf*dX*V[i]/2/h/100;
            second[i]:=Cd/b/h*Vjet(x[i])/100*(Ajet1*(Vjet(x[i])/V[i]-1)-Ajet2);
            dV[i]:=first[i]+second[i];

            V[i+1]:=V[i]+dV[i];
            x[i+1]:=x[i]+dx/12/100;
            end;

     for i:=101 to 159 do
            begin
            first[i]:=-Cf*dX*V[i]/2/h;
            second[i]:=Cd*Vjet(x[i])/b/h*(Ajet1*(Vjet(x[i])/V[i]-1)-Ajet2);
            dV[i]:=first[i]+second[i];

            V[i+1]:=V[i]+dV[i];
            x[i+1]:=x[i]+dx/12;
            end;

for i:=0 to 159 do
writeln ('X[',i,']= ',x[i]*12:5:3,' ',V[i]:5:3);
assign(f1,'a:\other\v_track.dat');
rewrite(f1);

for i:=0 to 53 do
    writeln(f1,x[i*3]*12:5:3,' ',V[i*3]:5:3);
close(f1);
end.
```

PROGRAM 4

```
{ THIS PROGRAM CALCULATES THE CAN SPEED IN FUNCTION OF THE CAN POSITION }
{ ON THE CONVEYOR                                                       }


program speed_calc;

const
Rho=0.07672;                    { specific weight of air (lbm/ft^3)          }
Cd=1;                           { drag coefficient for cylinder of H/D=1.84 }
L=9.5;                          { length of the conveyor (ft)                }
s=2;                            { spacing between two holes (in)             }
H=4.8;                          { height of the can (in)                     }
DIA=2.6;                        { diameter of the can (in)                   }
m=0.02645;                      { mass of one can (lbm)                      }


var
i,j,k,N,laststep:integer;
Dt,SumF,Af,Drag,F,FF,h_p0:real;
XC,V: array [0..3000] of real;
XH,FS:array [0..100] of real;
f1:text;

Function Fstat(x:real):real;    { interpolation of the experimental      }
const                           { data for Fx with a Lagrange polynomial }
a0=1.82876;
a1=0.487626;
a2=-0.561608;
a3=-0.112715;
a4=-0.546328;
a5=0.641491;
a6=-0.215378;
a7=0.019792;
a8=0.0010567;
var x3:real;
begin
x3:=x*x*x;
Fstat:=a0+a1*x+a2*x*x+a3*x3+a4*x*x3+a5*x*x*x3+a6*x3*x3+a7*x*x3*x3+a8*x*x*x3*x3;
end;


Function V_air(X:real):real;
const

b0=5.29;
b1=0.932;        (* this polynomial interpolates data of Vair above  *)
b2=-0.02576;     (* the deck plate calculated by Program 3           *)
b3=0.00041;      (* The conditions are : 2 sections of conveyor and  *)
b4=-3.15e-6;     (* Vair initial = 5 ft/s                            *)
b5=9.14e-9;

v_air:=b0+b1*X+b2*X*X+b3*X*X*X+b4*X*X*X*X+b5*X*X*X*X*X;

end;


function Vjet(x:real):real;  { The velocity of the air jets depends on      }
var                          { the pressure distribution in the plenum      }
P0:real;                     { The data for the pressure P0 are experimental}
```

```
begin
if ( (x>=0) and (x<6) )
   then P0:=1.95 else
if ( (x>=6) and (x<18) )
   then P0:=-8.333e-3*x+1.97 else
if ( (x>=18) and (x<30) )
   then P0:=-0.02*x+2.18 else
if ( (x>=30) and (x<42) )
   then P0:=8.33e-3*x+1.33 else
if ( (x>=42) and (x<54) )
   then P0:=1.68 else
if ( (x>=54) and (x<66) )
   then P0:=1.66e-3*x+1.59 else
if ( (x>=66) and (x<78) )
   then P0:=-0.0025*x+1.865 else
if ( (x>=78) and (x<90) )
   then P0:=9.16e-3*x+0.955 else
if ( (x>=90) and (x<102) )
   then P0:=1.66e-3*x+1.63 else
if ( (x>=102) and (x<=120) )
   then P0:=3.33e-3*x+1.46;


Vjet:=sqrt(2*5.2*32.2/rho*(P0-0.265));


end;


begin

write('what is the time interval (s) ? ');     { choice of the time interval }
readln (Dt);

N:=trunc(L*12/s);                              { N is the number of holes    }


XH[0]:=0;
For j:=1 to N do                               { XH is the position of the   }
    XH[j]:=XH[j-1]+2;                          { holes on the conveyor       }

i:=0;
XC[0]:=0;                                    { The can front is above 1st hole}
V[0]:=0;                                     { It starts moving with no speed }
Repeat
      SumF:=0;
      For j:=0 to N do                       { test for the can position      }
          begin
          if (( (XC[i]-XH[j])>3 ) or ( (XC[i]-XH[j])<-0.9 )) then
            FS[j]:=0.0
          else FS[j]:=Fstat(XC[i]-XH[j])*1e-3/0.454;      { jet force (lbm)  }
          SumF:=SumF+FS[j];
          end;
      F:=(Vjet(XC[i])-V[i])/Vjet(XC[i]) * SumF;       { total jet force (lbm) }

      Af:=DIA*H/144;                             { frontal area of the can (ft^2)}
      if ((V[i]-V_air(XC[i])) >=0 ) then
         Drag:=Cd*0.5*Rho*sqr(V[i]-V_air(XC[i]))* Af / 32.2  {drag force (lbf)}
      else Drag:=-Cd*0.5*Rho*sqr(V[i]-V_air(XC[i]))* Af / 32.2;
```

```
      FF:=F - Drag ;                                  { actual force (lbf)        }

      V[i+1]:=FF/m*32.2*Dt + V[i];                    { can speed (ft/s)          }

      XC[i+1]:= XC[i] + V[i+1]*Dt*12;                 { new can position (in)     }

      write ('V_air=',V_air(XC[i]):5:2);
      write ('  XC[',i+1,']=',XC[i+1]:5:1);           {screen display when running}
      writeln('   V[',i+1,']=',V[i+1]:5:2);          { ft/s }

      i:=i+1

                                                  { end of the loop as the center }
until XC[i] >= XH[N];                             { of the can is right above the }
                                                  { last hole                     }


writeln('the number of holes is : ', N);
writeln('the can passes through ',i,' positions ');
writeln('The velocity at the end (',L:3:1,' ft) is : ',V[i]:7:4,' ft/s');

laststep:=i-1;
assign(f1,'A:\other\spd1sV2.dat');
rewrite(f1);
for k:=0 to laststep do
            writeln (f1,k*Dt:4:2,' ',XC[k]:6:2,' ',V[k]:7:4);
close (f1);
end.
```

VITA

Sylvaine Chardon was born on July 3, 1968, in Fontainebleau, France. After graduating from High School in Fontainebleau in 1986, she prepared the entrance examination for the "Grandes Ecoles" during two years. In Fall 1988, she joined the Chemical Engineering Department at the "Université de Technologie de Compiègne" (U.T.C., France). While still in Compiègne, she participated in the U.T.C. - Virginia Tech exchange program to enroll in the Master Program at VPI & SU in Mechanical Engineering. After completing the requirements for a Master's degree at Virginia Tech, the author will seek employment in France.

Sylvaine L. Chardon